

A prevalent population of normal-mass central black holes in high-redshift massive galaxies

Junyao Li^{1*}, Yue Shen^{1,2} and Ming-Yang Zhuang¹

^{1*}Department of Astronomy, University of Illinois at Urbana-Champaign, Urbana, 61801, IL, USA.

²National Center for Supercomputing Applications, University of Illinois at Urbana-Champaign, Urbana, 61801, IL, USA.

*Corresponding author(s). E-mail(s): junyaoli@illinois.edu;

Understanding the co-evolution between supermassive black holes (SMBHs) and their host galaxies provides crucial insights into SMBH formation and galaxy assembly in these cosmic ecosystems [1]. However, measuring this co-evolution, as traced by the black hole mass - stellar mass relation towards the early Universe, often suffers from significant sample selection biases [2–6]. Samples selected based on the luminosity of the SMBH would preferentially find overly massive black holes relative to their host stellar mass, missing the population of lower-mass SMBHs that are underrepresented. Here we report the discovery of 13 moderate-luminosity broad-line Active Galactic Nuclei from a galaxy-based selection of 52 massive galaxies at $z \sim 3 - 5$. The derived SMBH masses for these AGNs yield a mean SMBH-to-stellar mass ratio of $\sim 0.1\%$, consistent with the local value [7]. There is limited evolution in this mean mass ratio traced back to $z \sim 6$, indicating that a significant population of “normal” SMBHs already existed within the first billion years of the Universe. Combined with the previous sample of overmassive black holes, there must be diverse pathways for SMBH formation in high-redshift galaxies. Most of these galaxies are experiencing star formation quenching by the observed epoch, suggesting the formation of massive quiescent galaxies does not necessarily require an overly massive black hole, contrary to some theoretical predictions [8–10].

Since the discovery of the tight correlation between SMBH mass and their host galaxy properties (e.g., stellar velocity dispersion, bulge mass) in the local universe, it has been suggested that the formation and evolution of galaxies and their central SMBHs are closely coupled [1, 7]. However, the origin of SMBHs and the physical mechanisms responsible for establishing these scaling relations is far from clear [11]. Theoretical models propose that AGN-driven outflows and jets inject substantial energy and momentum into the interstellar medium, self-regulating BH feeding and star formation, thereby fostering their coevolution [12]. Alternatively, the observed scaling relations may arise from non-causal processes, where frequent galaxy mergers and statistical averaging via the central limit theorem produce the observed local correlations [13, 14].

Semi-analytic models and cosmological simulations incorporating various BH seeding models, AGN and supernova feedback recipes, and merger histories predict different evolutionary tracks for the SMBH mass - stellar mass ($\mathcal{M}_{\text{BH}} - \mathcal{M}_\star$) relation, providing potential avenues to observationally constrain the seeding mechanisms of SMBHs and disentangle their coevolution pathways with galaxies [8, 15–20]. The launch of the James Webb Space Telescope (JWST) has transformed this field by enabling the detection of stellar emission from Active Galactic Nuclei (AGNs) at $z > 4$ for the first time, a critical epoch where simulation predictions diverge most significantly [8, 15]. Notably, high-redshift AGNs, spanning from relatively faint little dots (LDs¹) in low-mass galaxies ($\mathcal{M}_\star \lesssim 10^{10} M_\odot$), to the most luminous quasars in massive galaxies ($\mathcal{M}_\star \gtrsim 10^{10} M_\odot$), have been consistently observed to lie above the mean local $\mathcal{M}_{\text{BH}} - \mathcal{M}_\star$ relation by more than ~ 1 dex (i.e., overmassive BHs) [3, 4, 22, 23]. These findings have been interpreted as evidence that SMBHs predominantly originated from heavy seeds via direct collapse BHs ($M_{\text{seed}} > 10^5 M_\odot$), which initially lacked a stellar component [24].

However, most of these high-redshift samples are selected based on AGN luminosity, which would preferentially select more luminous and therefore more massive BHs in the more abundant low-mass galaxies. This statistical bias, known as the Lauer bias [25], could largely explain the elevated and flattened $\mathcal{M}_{\text{BH}} - \mathcal{M}_\star$ relation at early epochs [2, 6, 26]. Indeed, high-redshift shallow quasar surveys exclusively target AGN-dominated systems [27] thus overly massive BHs. On the other hand, deep pencil-beam JWST surveys would still predominantly select overmassive AGNs in the vastly more numerous low-mass galaxies [6], as high-mass galaxies with similar BH masses and AGN luminosities (but lower $\mathcal{M}_{\text{BH}}/\mathcal{M}_\star$) at the same detection limit are much rarer in these small fields.

To remedy for selection biases in previous overmassive AGN samples and search for the potential presence of normal and undermassive BHs (defined as those located on and below the mean local relation) at early cosmic times, we specifically search for faint broad-emission-line (BL) AGNs in massive high-redshift galaxies from deep JWST surveys, and measure the $\mathcal{M}_{\text{BH}}/\mathcal{M}_\star$ ratio therein. The presence of broad emission lines is a prerequisite for BH mass estimation [28, 29]. Here we report the identification of 13 BLAGNs at $z > 3$. Their BH masses and AGN luminosities are comparable to

¹In this paper, LDs refer to high-redshift ($z > 4$) faint AGNs with compact host galaxies and overmassive BHs discovered in deep JWST surveys [3, 4, 21].

overmassive LDs, but they are hosted in massive galaxies. While their stellar masses are similar to those of quasars, their BH masses are up to ~ 3 orders of magnitude lower (Fig. 1). The average $\mathcal{M}_{\text{BH}}/\mathcal{M}_*$ ratio ($\sim 0.1\%$) of these BLAGNs is consistent with the local value [7], demonstrating that high-redshift SMBHs are not universally overmassive to their stellar component, as inferred from previous biased samples [10]. Instead, a significant population of normal BHs has been overlooked.

Our AGN samples were identified through a systematic search for broad $\text{H}\alpha$ emitters among spectroscopically confirmed massive galaxies at $z \sim 3 - 5$ across six deep JWST fields covered by the ASTRODEEP catalog [30]. The combined large survey area ($\sim 0.2 \text{ deg}^2$) was crucial for improving the statistics of rare massive galaxies hosting normal BHs. Stellar masses were derived using prism spectroscopy from the JWST Near Infrared Spectrograph (NIRSpec), combined with photometry from multiple Hubble Space Telescope (HST) and JWST Near-Infrared Camera (NIRCam) surveys (Methods). The rest-frame $\sim 0.2 - 1.0 \mu\text{m}$ coverage provided by NIRSpec enables robust \mathcal{M}_* measurements through spectral energy distribution (SED) fitting which accounts for AGN contamination (see Methods). Among the 92 massive galaxies with $\mathcal{M}_* > 10^{10} M_\odot$ and $z \sim 3 - 5$ identified in ASTRODEEP, 52 were observed with NIRSpec in medium-to-high resolution mode ($R \sim 1000 - 5000$) covering the $\text{H}\alpha$ line, which defines our parent galaxy sample for BLAGN identification. This approach differs from selection techniques that require an AGN-dominated continuum (e.g., color-selected quasars; [5, 22, 23]), and thus remedies for the Lauer bias.

As detailed in Methods, BLAGNs were identified by detecting broad $\text{H}\alpha$ emission with a full-width-at-half-maximum (FWHM) exceeding 1000 km s^{-1} through spectral decomposition in the $\text{H}\alpha + [\text{N II}] + [\text{S II}]$ region. Additional model assessments were performed to differentiate line broadening in the broad-line region (BLR) from that caused by outflows. A total of 14 BLAGNs were identified from the 52 galaxies, suggesting that AGN activity is prevalent in high-redshift massive galaxies. Extended Fig. 2 presents the spectral decomposition results. The bolometric luminosities (L_{bol}) and BH masses of these AGNs were estimated using the single-epoch virial estimator based on the width and extinction-corrected luminosity of the decomposed broad $\text{H}\alpha$ component [31, 32]. Extended Table 2 summarizes the derived stellar masses, BH masses, bolometric luminosities, and emission line properties.

Among the 14 BLAGNs, 16713-CEERS with $\log L_{\text{bol}} \sim 45.9 \text{ erg s}^{-1}$ stands out with an extremely broad $\text{H}\alpha$ (FWHM $\sim 9000 \text{ km s}^{-1}$), corresponding to $\log \mathcal{M}_{\text{BH}}/M_\odot \sim 9.1$ and $\mathcal{M}_{\text{BH}}/\mathcal{M}_* \sim 10\%$, resembling overmassive quasars at $z \sim 6$ [22, 23]. The remaining 13 sources exhibit moderate BH masses ($\log \mathcal{M}_{\text{BH}}/M_\odot \sim 6.6 - 8.1$) and luminosities ($\log L_{\text{bol}}/\text{erg s}^{-1} \sim 44.2 - 45.3$), comparable to LDs at slightly higher redshifts ($z \sim 5$). The prominent Balmer break, 4000 Å break, stellar absorption features, and/or red UV-optical continuum shape observed in the prism spectroscopy for most galaxies (see Extended Fig. 1) indicate that the continuum emission is not dominated by the BLAGN but a significant population of old, evolved stars. The decomposed AGN flux fraction is typically $f_{\text{AGN}} \sim 15\%$ (Methods). This is fundamentally different from LDs, which exhibit a blue, AGN-dominated UV-optical continuum [3].

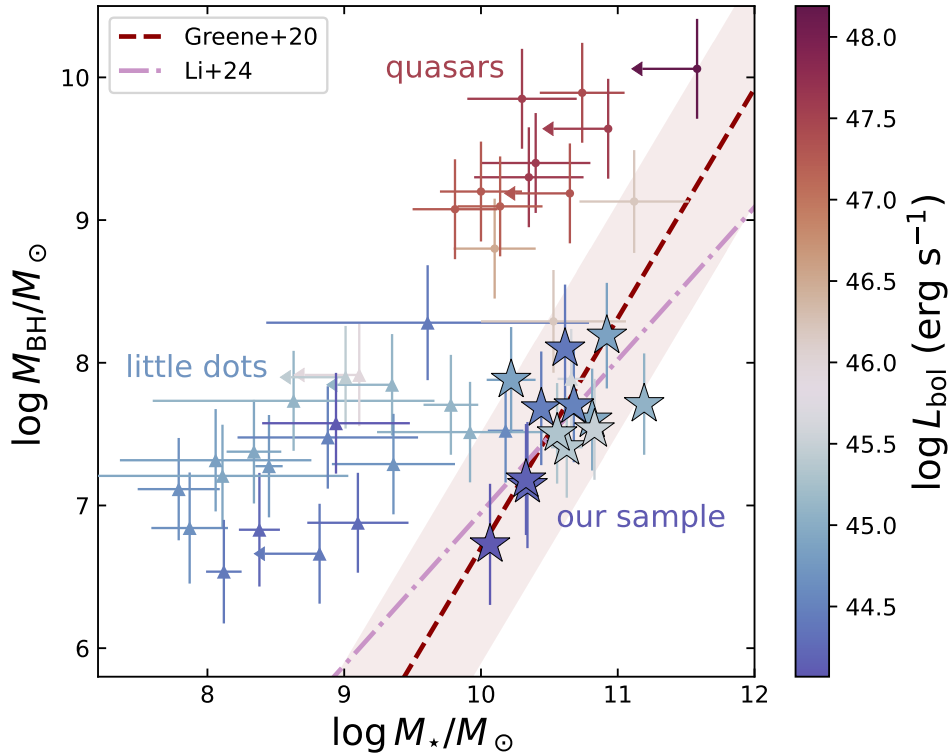


Fig. 1 The distribution of high redshift AGNs in the $\mathcal{M}_{\text{BH}} - \mathcal{M}_*$ plane. The stars represent the 13 faint BLAGNs at $z \sim 3 - 4$ identified in this work. The circles denote $z \sim 6$ quasars from [5], [22], and [23], while the triangles indicate faint LDs at $z \sim 4 - 7$ identified in the JADES and CEERS surveys by [3] and [4]. Each data point is color-coded by the AGN luminosity. For comparison, the local $\mathcal{M}_{\text{BH}} - \mathcal{M}_*$ relation from [7] based on their combined fit for all galaxy types is shown as the red dashed line, with its intrinsic scatter (~ 0.81 dex) depicted as the red shaded region. The high-redshift intrinsic $\mathcal{M}_{\text{BH}} - \mathcal{M}_*$ relation, derived by correcting observational biases of LDs from [6], is shown as the pink dash-dotted line. The literature samples are recalibrated using the [31] recipe for $\text{H}\alpha$ -based BH mass measurements and the [32] relation for $\text{H}\alpha$ -based bolometric luminosity measurements, as for our own sample.

Fig. 1 shows the distribution of the 13 relatively faint AGNs (excluding aforementioned 16713-CEERS) in the $\mathcal{M}_{\text{BH}} - \mathcal{M}_*$ plane, color-coded by AGN luminosity. They form a distinct locus centered on the local $\mathcal{M}_{\text{BH}} - \mathcal{M}_*$ relation [7] with $\mathcal{M}_{\text{BH}}/\mathcal{M}_* \sim 0.1\%$ on average, in contrast to LDs and quasars, which are significantly elevated to the upper envelope of the local relation with $\mathcal{M}_{\text{BH}}/\mathcal{M}_* \sim 10\%$ [3, 4, 22, 23]. Although our sample, drawn from multiple NIRSspec surveys, is incomplete and non-uniform (see Methods), this comparison demonstrates clear selection biases in previous samples caused by the finite AGN detection limit. Shallow and wide-area quasar surveys, with a typical luminosity limit of $L_{\text{bol}} \gtrsim 10^{46}$ erg s^{-1} [22, 23], fail to detect low-mass BHs in high-mass host galaxies due to their faintness. On the other hand, deep pencil-beam JWST surveys can detect faint AGN luminosities to

$L_{\text{bol}} \gtrsim 10^{44}$ erg s $^{-1}$ at $z > 3$, but the detected population will be dominated by LDs in the more numerous low-mass host galaxies than high-mass galaxies due to the Lauer bias². In fact, the handful of LDs residing in high-mass ($\mathcal{M}_* > 10^{10} M_\odot$) galaxies from previous samples follow the mean local $\mathcal{M}_{\text{BH}}/\mathcal{M}_*$ ratio (Fig. 1), as the JWST limit is sufficient to detect normal-mass BHs at these high stellar masses.

With our dedicated sample selection, the statistics in the high- \mathcal{M}_* , low- \mathcal{M}_{BH} regime are now robust. Notably, our sample aligns with the high-redshift mass relation reported by [6], which used forward modeling to correct observational biases in the LD sample and infer their intrinsic mass relation. Nevertheless, even lower-mass BHs with fainter luminosities ($L_{\text{bol}} < 10^{44}$ erg s $^{-1}$) and narrower line widths (FWHM < 1000 km s $^{-1}$) may still be missed in our search.

The reconstructed star formation history (SFH) of the 13 faint AGN systems derived using a delayed- τ model (star formation rate $\propto t \exp(-t/\tau)$) is shown in Fig. 2 (see Methods for details and additional model tests). Thanks to the faintness of the central AGN, we are able to obtain more accurate constraints on their host galaxy properties compared to overmassive LDs and quasars. The stellar mass of most systems was assembled during an active star-forming period at $z > 5$, followed by a significant decline in star-forming activity within the past ~ 1 Gyr. The quenching nature of most galaxies in our sample is evident from their red spectral shape, which resembles that of post-starburst galaxies and quiescent galaxies (Extended Fig. 1). This aligns with recent findings that a significant population of massive galaxies at these epochs was assembled very early and became quenched, with widespread AGN activity likely playing a significant role [33–36].

It is unclear if the prevalence of quiescent galaxies among our BLAGNs is due to additional selection biases in the heterogeneous parent galaxy sample. Many JWST NIRSspec observations, such as RUBIES [37] and JADES [38], prioritize red, bright, and rare objects during shutter allocation. While the preference for red objects introduces a bias against star-forming and AGN-dominated systems, such blue galaxies may still dominate the bright population. Even if the parent galaxy sample is somewhat biased towards the quiescent population, it offers a unique opportunity to search for normal-mass or undermassive BHs at $z > 3$ – that is, faint AGNs contribute negligibly to the continuum emission but dominate the line emission, which would otherwise be outshined in luminous, massive star-forming galaxies.

Since most systems assembled the bulk of their stellar mass at $z > 5$, we can place a strong constraint on the upper limit of their $\mathcal{M}_{\text{BH}}/\mathcal{M}_*$ ratios back to $z = 5.7$, the mean redshift of current high- z LDs and quasars, to investigate the evolutionary pathways of different populations within the first billion years of the Universe. This is achieved by deriving the stellar mass decrement from the SFH while assuming the BH mass remains constant over time. As shown in Fig. 2, changes in \mathcal{M}_* (~ 0.15 dex) and $\mathcal{M}_{\text{BH}}/\mathcal{M}_*$ are minimal for the ten objects with formation redshifts (defined as the epoch when half of the stellar mass was formed) greater than $z = 5.7$. Given that the BH mass must also decrease with increasing lookback time, this analysis suggests that a significant population of normal-mass or even undermassive BHs, both following and

²This argument assumes a positive intrinsic $\mathcal{M}_{\text{BH}} - \mathcal{M}_*$ relation and a relatively mass-independent Eddington ratio distribution.

below the mean local relation, were already in place within the first billion years of the universe.

Several factors would complicate the direct detection of such low-mass objects in the reionization era. At these epochs, the host galaxies are still actively forming stars, with spectral shapes resemble those of blue AGNs [3, 39]. This similarity makes it challenging to disentangle AGN and stellar components for robust stellar mass measurements, especially considering that NIRSpect observations are limited to rest-frame UV-optical emission at $z > 6$. Additionally, the outshining of young stars over old stellar populations can lead to an underestimation of stellar mass [40, 41]. Starburst-driven outflows can further hinder the identification of a BLR component, whose line width is expected to be even narrower due to the decreasing BH mass. Nevertheless, our reconstructed SFH suggests that such objects must be prevalent at $z > 6$ and are yet to be discovered.

Importantly, the distinct BH mass and stellar mass ranges observed for LDs, quasars, and our faint BLAGNs when back-traced to $z \sim 6$ suggest that diverse formation channels and evolutionary pathways for SMBHs must be at work in the early Universe. LDs and the most-luminous quasars likely originate from heavy seeds [24], with overmassive BHs capable of rapidly quenching their compact host galaxies [42], and potentially evolving into the cores of present-day elliptical galaxies [43]. In contrast, normal- and low-mass BHs in massive galaxies may have formed from lighter seeds, whose subsequent growth was impeded until their hosts could accumulate sufficient bulge mass to deepen the potential well to withhold the cold gas that would otherwise be blown off by supernova feedback. This cold gas can then be transferred into the nuclear region to feed the BH growth [7, 44, 45]. These diverse populations imply that a combination of seeding mechanisms, feedback processes, and mergers, rather than a single formation channel inferred from individual biased samples, has shaped the relations between SMBHs and galaxies as observed today.

Fig. 2 compares the offset of our sample from the local mass relation with predictions from four cosmological simulations – ASTRID, TNG300, Horizon-AGN, EAGLE – and the Dark Sage semi-analytic model, calibrated at $\log \mathcal{M}_* \sim 10.5$ [8, 15, 46]. Literature LDs and quasar samples are also shown for comparison. Previous overmassive quasar samples ($\log \mathcal{M}_*/M_\odot \sim 10.5$ and $\mathcal{M}_{\text{BH}}/\mathcal{M}_* \sim 10\%$), which are significant outliers to the underlying BH populations, are in tension with all simulations. In contrast, the missing normal BHs discovered in our study agree with most theoretical models that predict a much slower $\mathcal{M}_{\text{BH}}/\mathcal{M}_*$ evolution over cosmic time. Our result clearly demonstrates that selection biases can completely hide the intrinsic mass relation and mislead theoretical models. However, given the complex target selection criteria of our parent galaxy sample, we cannot robustly constrain the mean and scatter of the mass relation or distinguish between model predictions. Future JWST spectroscopic surveys with more uniform selection functions (e.g., [47]) will enable tighter and less biased constraints on the evolution of the mass relation and provide further insights into the physics of BH seeding and AGN feedback (e.g., [17]).

Despite producing a slowly-evolving mean $\mathcal{M}_{\text{BH}}/\mathcal{M}_*$ ratio, these state-of-the-art cosmological simulations often struggle to reproduce the large population of high-redshift massive quiescent galaxies found by JWST [9, 48]. These simulations often

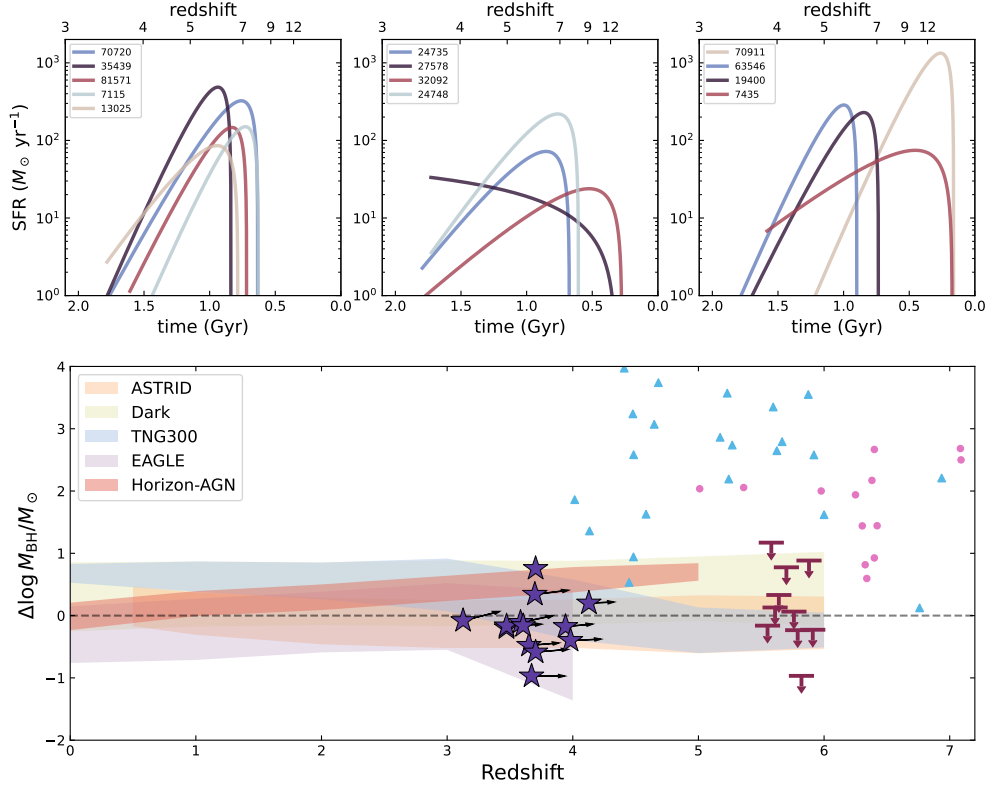


Fig. 2 Tracing the evolution of the SMBH-to-stellar mass ratio for the 13 faint BLAGNs. **Top:** The reconstructed SFH of the 13 faint BLAGNs using a delayed- τ model (Methods). **Bottom:** The offset in BH mass relative to the mean local relation in [7] for the 13 faint BLAGNs at their observed redshifts (stars). The upper limits of the back-traced offset at $z = 5.7$ (i.e., the mean redshift of LDs and quasars) for the 10 faint AGNs with formation redshifts greater than 5.7 are shown as red arrows, slightly shuffled in redshift for better visualization. The black arrows next to the stars represent the back-traced evolution trajectory. The predicted offsets (16th – 84th percentile) at $\log \mathcal{M}_*/M_\odot = 10.5$ in five cosmological simulations and semi-analytic models [8, 15] are shown in shaded bands. Literature quasar samples (pink circles with $\log \mathcal{M}_*/M_\odot \sim 10.5$; [5, 22, 23]) and faint LDs (cyan triangles with $\log \mathcal{M}_*/M_\odot \sim 8.5$; [3, 4]) are plotted for comparison.

require an overmassive black hole as an efficient driver of galaxy-wide star formation quenching [8, 9]. However, the host galaxies experiencing star formation quenching in our sample, which have $\mathcal{M}_{\text{BH}} \lesssim 10^8 M_\odot$ and $\mathcal{M}_{\text{BH}}/\mathcal{M}_* \sim 0.1\%$, are at odds with several model assumptions and predictions regarding the prerequisite for AGN quenching. For instance, in the ASTRID simulation, the kinetic feedback mode in low accretion rate AGNs – primarily responsible for massive galaxy quenching by preventing gas cooling in the circumgalactic medium – is activated only when $\mathcal{M}_{\text{BH}}/M_\odot > 10^{8.5} M_\odot$ at $z < 2.3$, whereas the thermal feedback mode implemented at $z > 2.3$ fails to effectively quench massive galaxies [8, 46]. A similar trend is observed in IllustrisTNG, where massive quenched galaxies at $z \sim 3$ exclusively host overmassive BHs with

$\log \mathcal{M}_{\text{BH}} > 8.5$ [9]. The analytic model proposed in [10] relates quenching to the $\mathcal{M}_{\text{BH}}/\mathcal{M}_*$ ratio, yet its predicted quenching threshold for high-redshift massive galaxies ($\mathcal{M}_{\text{BH}}/\mathcal{M}_* \sim 1\%$) is an order of magnitude higher than our observations, once we substitute our mean Eddington ratio ($\lambda_{\text{Edd}} \sim 0.1$) in their model.

Our results thus suggest that additional quenching mechanisms, not relying on overmassive BHs, are required to enable more efficient star formation quenching in simulations in order to reconcile with recent JWST observations of high-redshift massive quiescent galaxies [9, 48]. This could involve more effective supernova feedback and starburst-driven outflows than those currently implemented in cosmological simulations [49], or more efficient AGN feedback in the low BH mass regime. After quenching, stellar winds from old, evolved stars could become a major source of BH fueling. This effective growth channel, along with merging with other galaxies hosting overmassive BHs, may gradually establish the $\mathcal{M}_{\text{BH}} - \mathcal{M}_*$ relation for local ellipticals [1, 14, 50], and could explain the prevalence of AGN activity in quiescent galaxies [36, 50]. Ultimately, radio-mode feedback could be triggered in these fully grown massive BHs and sustain long-term quiescence of the host. Future spatially resolved studies of the stellar population, kinematics, outflows, radio activity, residual star formation and gas reservoir in our sample will provide critical insights into their formation history and inform upcoming high-resolution cosmological simulations.

Methods

Cosmological model

The cosmological parameters used in this paper are $H_0 = 70 \text{ km s}^{-1} \text{ Mpc}^{-1}$, $\Omega_m = 0.3$, and $\Omega_\Lambda = 0.7$. The Chabrier initial mass function (IMF) [51] is adopted to estimate stellar masses to be consistent with the literature AGN samples shown in Fig. 1. Magnitudes are given in the AB system.

Spectroscopic data

The spectroscopic data used to identify high-redshift massive galaxies and BLAGNs are from the DAWN JWST Archive (DJA³). As of January 8, 2025, DJA reduced the NIRSpec Microshutter Array (MSA) spectroscopy using the latest version of `msaexp` [37, 52, 53] and publicly released the version 3 data⁴ for 43 programs.

The detailed MSA data reduction procedures using `msaexp` are described in [37, 53]. For the DJA data release v3, pipeline version 1.14.0 and calibration files `jwst_1225.pmap` from the Calibration Reference Data System were used. In addition to the standard JWST pipeline calibration steps, `msaexp` applies updated corrections for MSA bar vignetting and improves sky background subtraction by differencing 2D spectra from different nod positions. The cross-dispersion profile for each source is fitted with curved 2D traces, accounting for spatial offset, width, and the wavelength-dependent point spread function (PSF). The 2D profile is then rectified for optimally weighted 1D spectral extraction using the algorithms in [54]. `msaexp` also applies a path-loss correction by fitting the source with a Gaussian profile that considers its position within the slit.

The absolute flux calibration accuracy of NIRSpec MSA spectroscopy is typically at the $\sim 10\% - 20\%$ level [37]. DJA also provides spectroscopic redshifts derived using the template fitting methods implemented in `msaexp`. The redshifts are visually inspected and graded for reliability, with a grade of 3 indicating a robust redshift.

Photometric data and slit loss correction

Although the flux calibration and path-loss correction have been significantly improved in the JWST MSA reduction pipeline and `msaexp`, which should be sufficient for compact sources, additional slit-loss corrections are required for extended sources to obtain accurate stellar mass measurements. In this study, we calibrate the prism spectroscopy for stellar mass measurements using the 16-band HST and JWST/NIR-Cam photometry ($0.44 \mu\text{m}$ to $4.44 \mu\text{m}$) from the ASTRODEEP catalog [30]. The photometric catalog covers six deep extra-galactic fields: Abell 2744, EGS, COSMOS, UDS, GOODS-S, and GOODS-N, with a total area of $\sim 0.2 \text{ deg}^2$. The exact number of available bands varies across fields, with a median of ~ 12 for our massive galaxy sample, as detailed below.

³<https://dawn-cph.github.io/dja/>

⁴<https://dawn-cph.github.io/dja/spectroscopy/nirspec/>

Source detection in ASTRODEEP was performed with **SExtractor** on a weighted stack of F356W and F444W images, achieving nearly 100% completeness at ~ 28 mag, which is sufficiently deep for massive galaxies at the redshift range considered in this study ($z \sim 3 - 5$). Aperture fluxes were extracted within diameters of $0.''2$ to $5.''3$ and corrected for galactic extinction. The elliptical isophote and Kron-like fluxes, which approximate the total flux well [55], were measured in the detection band. The aperture correction factor for this band was then scaled to other bands, assuming no color gradient dependence. For each field, ASTRODEEP provides an optimal catalog, where total fluxes are derived from colors measured in a preferred aperture based on the objects' segmentation map. We use these fluxes to calibrate our prism spectra.

For each object, we generate synthetic photometry by convolving the filter transmission curve with the prism spectra in photometric bands with signal-to-noise ratio (SNR) > 3 in ASTRODEEP. We then compute the flux ratio between the synthetic and observed photometry and fit it as a function of wavelength using an n -th order polynomial. By default, we set $n = 3$ in the fitting and adjust it between 0 and 5 as needed. Higher-order fits are used for poor residuals, while lower-order fits are adopted when fewer photometric bands are available for calibration. The fitting result is visually inspected to ensure that high-order fits do not introduce artificial changes to the spectral shape. The derived calibration term is then applied to the prism data, yielding fully flux-calibrated spectra. The median correction factor is 1.05, 1.13, 1.08, and 1.31 in F115W, F150W, F277W, and F444W, respectively.

The medium-to-high resolution NIRSpec spectroscopy used for BH mass measurements is corrected only with the default `msaexp` slit-loss routine and not further matched to the NIRCам photometry, which includes significant contributions from the stellar component in massive galaxies. Since $\log \mathcal{M}_{\text{BH}} \propto 0.47 \log L_{\text{bol}}$ [31], a 50% flux loss from the central point source would only affect the derived BH mass by ~ 0.14 dex, which is much smaller than the uncertainty inherent in the BH mass estimator (~ 0.4 dex; [29]).

Identifying massive galaxies with SED fitting

We begin with the spectroscopically confirmed galaxies in DJA to define the parent sample of high-redshift massive galaxies for BLAGN identification. Galaxies are selected at $3 < z < 5$ with robust spectroscopic redshifts (grade 3), a median SNR > 10 for the prism spectra, no significant spectra gap, and must lie within the ASTRODEEP fields for spectral calibration purpose. The upper redshift limit ensures rest-frame near-infrared coverage by NIRSpec, which is essential for accurate stellar mass measurements [56]. These criteria results in 399 galaxies from the following programs: 1180, 1181 (PI: D. Eisenstein; [38, 57]), 1199 (PI: M. Stiavelli; [58]), 1210, 1212, 1213, 1214, 1215, 1286 (PI: N. Luetzgendorf; [38]), 1211 (PI: K. Isaak; [59]), 1345 (PI: S. Finkelstein; [60]), 2198 (PI: L. Barrufet; [61]), 2561 (PI: I. Labbe; [62]), 2565 (PI: K. Glazebrook; [34]), 2750 (PI: P. Arrabal Haro; [63]), 2756 (PI: W. Chen), 2767 (PI: P. Kelly; [64]), 3073 (PI: M. Castellano; [65]), 3215 (PI: D. Eisenstein; [66]), 4233 (PI: A. de Graaff; [37]), 6541 (PI: E. Egami), 6585 (PI: D. Coulter). These programs are designed to address a wide range of science goals, with additional filler targets included

in the slits for ancillary science. As a result, quantifying the sample selection function is highly challenging.

We then measure their stellar masses using **CIGALE**, a multiwavelength SED fitting code with flexible AGN templates to model the AGN continuum emission [67]. **CIGALE** employs **SKIRTOR**, a clumpy two-phase torus model based on the 3D radiative transfer code **SKIRT**, to fit the direct, anisotropic accretion disk emission, described by wavelength-dependent broken power laws, along with the re-radiated infrared emissions from the surrounding clumpy torus. Additionally, it includes a separate dust extinction curve (we adopt the SMC curve; [68]), independent of the torus and host galaxy attenuation, to account for the polar dust component commonly observed in AGNs [69].

Since our goal is to measure the stellar mass of BLAGNs, we set the viewing angle to 30° , representing a type 1 configuration where the line of sight does not intersect the dusty torus, thus allowing a direct view of the BLR. In this configuration, the extinction of the AGN continuum is dominated by the polar dust component, with typical extinction up to $A_V \sim 1$ mag [70]. The strength of the AGN is controlled by a normalization factor f_{AGN} , which represents the flux ratio of the dust-extinguished AGN flux to the total flux at 5100 \AA . The remaining AGN parameters, such as dust emissivity and torus structure properties, are kept at their default values to avoid strong degeneracy. While the stellar mass estimates for type 2 AGNs may be inaccurate under this type 1 configuration, such objects will not enter our final BLAGN sample.

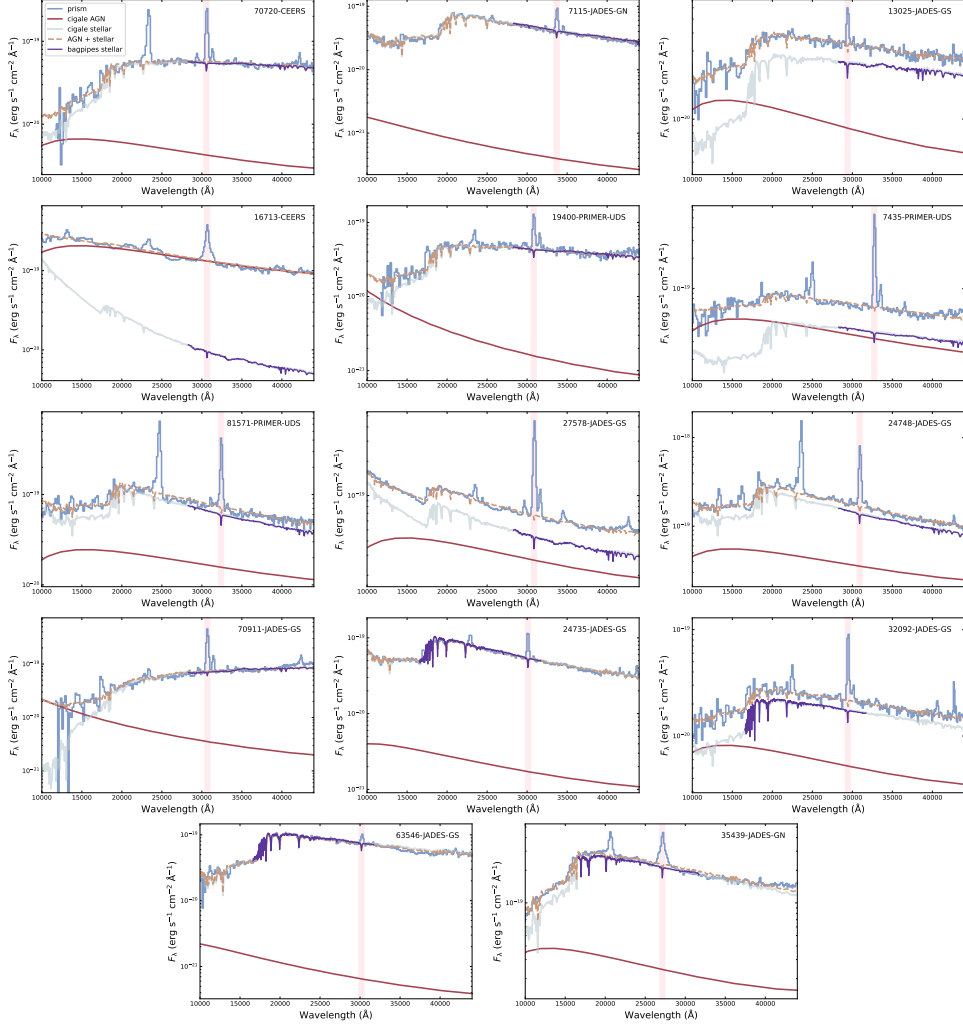
Due to potential contamination of the **ASTRODEEP** photometry by strong AGN emission lines, which cannot be properly fitted by **CIGALE**'s nebular line model, we mask emission lines in the calibrated prism spectra and extract continuum-only spectra using a median filter. Synthetic photometry is then generated from the continuum in 22 HST+JWST filters (F435W to F444W), effectively sampling the SED shape for stellar population modeling. The BC03 stellar population model [71], Chabrier initial mass function [51], Calzetti extinction law [72], and the delayed SFH, which best reproduces the stellar mass in **CIGALE** through extensive simulation tests [73], are adopted. Galactic dust emission is negligible at $\lambda_{\text{rest}} \lesssim 1 \mu\text{m}$ and is not included in our fitting.

Extended Table 1 summarizes the **CIGALE** parameters adopted in this study. In the fitting, we set the **additionalerror** parameter to 15% to account for uncertainties not captured by the flux errors in the spectroscopy and photometric catalogs. These include wavelength-dependent color gradients and galaxy structure in aperture corrections, continuum extraction using a median filter, and uncertainties in the polynomial fit used to calibrate the prism spectra. We verified that varying this parameter has a negligible impact on the derived stellar masses, although lower and higher values of **additionalerror** lead to decreased and increased mass uncertainties, respectively.

This SED fitting procedure identifies 92 massive galaxies with $\mathcal{M}_* > 10^{10} M_\odot$. Extended Fig. 1 demonstrates our SED decomposition method using the final sample of 14 BLAGNs as detailed below.

Table 1 SED fitting parameters in CIGALE. We first run CIGALE using a sparser grid, reduced by a factor of two compared to the table values, to identify massive galaxies. The selected massive galaxies ($M_* > 10^{10} M_\odot$) are then fitted with the listed parameters to obtain more accurate stellar mass estimates and their associated uncertainties.

Module	Parameter	Values
Star formation history: delayed model, $\text{SFR} \propto t \exp(-t/\tau)$	e -folding time, τ (Gyr)	0.1 - 7.0, step 0.05
	Stellar age, t (Gyr)	0.1 - 2.2, step 0.05
Simple stellar population: BC03 [71]	Initial mass function	Chabrier [51]
	Metallicity (Z)	0.004, 0.008, 0.02
Galactic dust attenuation: Calzetti+2000 [72]	$E(B - V)$ of the young population	0.0 - 1.0, step 0.05
	$E(B - V)$ ratio between the old and young populations	0.44
AGN: SKIRTOR	Torus optical depth at 9.7 microns $\tau_{9.7}$	7.0
	Torus density radial parameter	1.0
	Torus density angular parameter	1.0
	Angle between the equatorial plan and edge of the torus	40°
	Ratio of the maximum to minimum radii of the torus	20
	Viewing angle θ	30° (type 1)
	AGN fraction at 5100 Å	0.01 - 0.99, step 0.02
	Extinction law of polar dust	SMC
	$E(B - V)$ of polar dust	0.0 - 0.3, step 0.03
	Temperature of polar dust (K)	100
Emissivity of polar dust	1.6	



Extended Fig. 1 Decomposing the continuum SED into AGN and galaxy components for the final sample of 14 BLAGNs. The blue curves represent the flux-calibrated prism spectra. Emission lines were masked when generating the synthetic SEDs for CIGALE fitting. The red and gray curves show the best-fit AGN and stellar templates derived using CIGALE, respectively. The purple curve represents the resolution-matched stellar template in the medium-to-high resolution grating used to identify each BLAGN (see Extended Table 2), generated by Bagpipes [74]. The orange dashed curve represents the combined AGN and stellar models.

Spectral decomposition and broad-line AGN identification

Among the 92 massive galaxies, 52 objects have medium-to-high resolution spectroscopy obtained with the G235M, G235H, G395M, or/and G395H gratings covering the $H\alpha$ region. These objects constitute the parent galaxy sample for our BLAGN

search. BLAGNs are identified by detecting a broad $H\alpha$ component, after ruling out an outflow origin [3, 4, 75]. We use `lmfit` [76] for spectral decomposition and fitting quality assessment, which applies the Levenberg-Marquardt optimization algorithm to minimize the likelihood function. Since the data reduction pipeline typically underestimates the flux uncertainties, we compare the continuum scatter around the emission lines to the median value of the error spectrum in the same wavelength range. The error spectrum is then rescaled by their ratio.

The spectral fitting is restricted to 41 objects with $\text{SNR}(H\alpha + [N\text{II}]) > 20$ and starts with the default Model A, which consists of three Gaussian profiles for the $[N\text{II}]$ doublets and $H\alpha$. The flux ratio of $[N\text{II}]\lambda 6549$ and $[N\text{II}]\lambda 6585$ is fixed at the theoretical value of 1:2.9. The $[S\text{II}]\lambda 6718$ and $[S\text{II}]\lambda 6732$ doublets are fitted simultaneously to facilitate decomposition of $H\alpha$ and $[N\text{II}]$ if detected with $\text{SNR} > 5$, allowing a free flux ratio. All narrow lines are forced to have the same width and velocity offset. A broad Gaussian component, centered on the narrow $H\alpha$ line, is then added to represent the broad $H\alpha$ component ($H\alpha_{\text{b}}$; Model B). The Bayesian Information Criterion (BIC), defined as $\text{BIC} = \chi^2 + k \ln(n)$, where k is the number of free parameters and n is the number of data points, is used to evaluate the significance of the broad component under assumptions of Gaussian uncertainties. Detection of the broad component is deemed significant if $\text{FWHM}(\text{broad}) > 1000 \text{ km s}^{-1}$, $\text{FWHM}(\text{broad}) > 2 \times \text{FWHM}(\text{narrow})$, and the fit improves by $\Delta\text{BIC}(A - B) > 10$ [77].

However, the broad component is not necessarily related to the BLR, as it could arise from the superposition of the three outflow components associated with the narrow $H\alpha$ and $[N\text{II}]$ lines, although such cases are rare in recent JWST study of high-redshift AGNs [75]. To address this, an additional procedure is applied to sources with a detected broad $H\alpha$ component in the previous step. We first examine the $[S\text{II}]$ and $[O\text{III}]\lambda\lambda 4959, 5007$ lines if either is detected with $\text{SNR} > 5$. If an outflow component is identified in either line, evidenced by $\Delta\text{BIC} > 10$ when an additional Gaussian component improves the fit, a corresponding outflow component is included in the joint fit of all narrow lines around $H\alpha$ (Model C). The width, velocity offset, and relative flux ratio of the outflow component to the narrow core component are forced to be identical and cannot exceed those of $[O\text{III}]$, as outflow features are typically much weaker in $H\alpha$, $[N\text{II}]$ and $[S\text{II}]$ [78]. The presence of a BLR is then evaluated by adding a broad $H\alpha$ component centered on the narrow $H\alpha$ line (Model D), with $\Delta\text{BIC}(C - D) > 10$ required for detection. If no outflow component is detected in $[S\text{II}]$ or $[O\text{III}]$, the presence of a BLR is claimed. In cases where $[O\text{III}]$ and $[S\text{II}]$ are undetected or not covered, Model B with few parameters is preferred over Model C if it yields a lower BIC value, indicating no evidence for outflows and supporting the BLR interpretation [75].

Each line is convolved with the line spread function (LSF) in the fitting. The LSF provided by `JDOX` is valid only for uniformly illuminated sources, which significantly underestimates the actual spectral resolution [3, 79]. Therefore, we use `msafit` to model the LSF, which measures the realistic spectral resolution by forward modeling

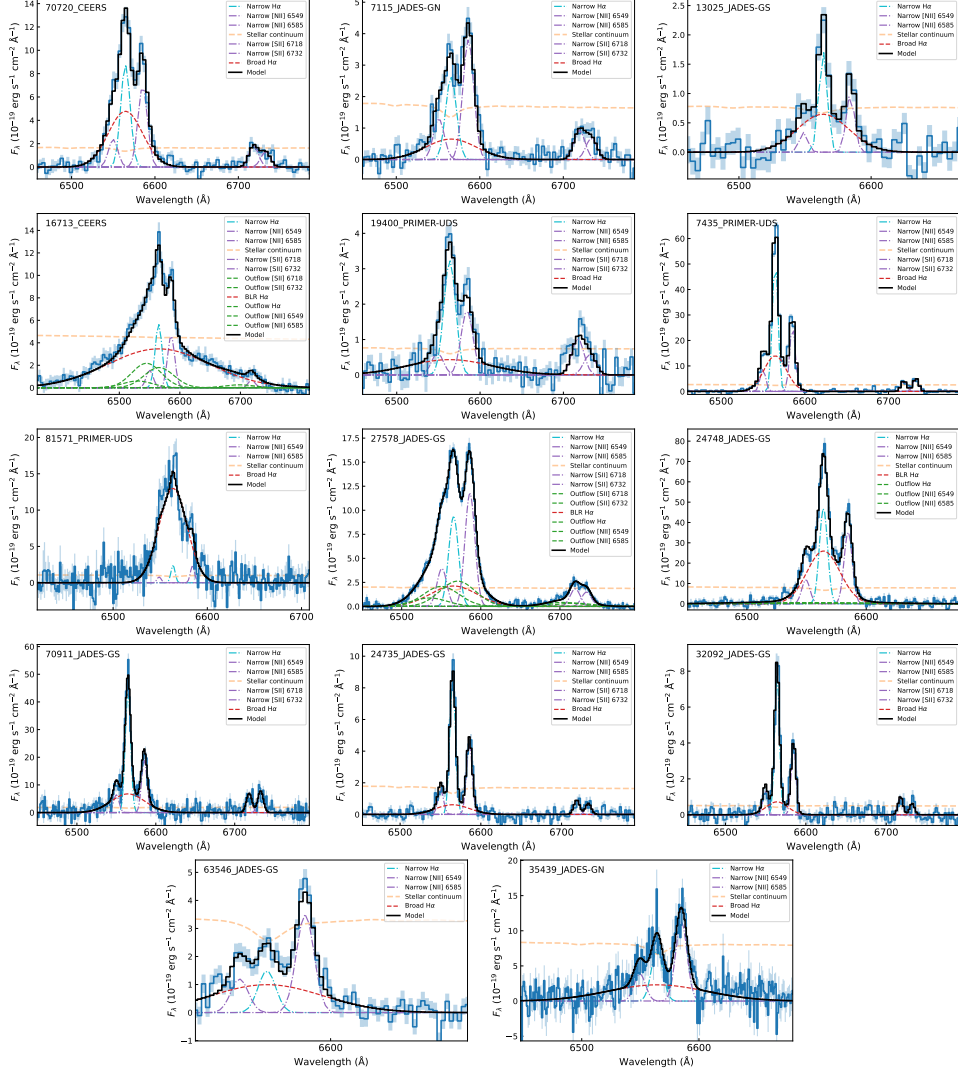
the light trajectory on the JWST detector for a given source position [79]. As a reference, the typical resolution for the H α line in the G235M, G235H, G395M, G395H gratings is 150 km s $^{-1}$, 50 km s $^{-1}$, 200 km s $^{-1}$, and 80 km s $^{-1}$, respectively.

The continuum model is adopted from SED fitting, which accounts for the impact of Balmer absorption on the observed emission line profile, significant in many massive galaxies. Since the SED model produced by CIGALE has low spectral resolution, we use Bagpipes [74] to generate the stellar continuum at a resolution matched to the NIRSpect gratings. The best-fit stellar parameters from CIGALE and the LSF obtained using msafit are provided as inputs to the model_galaxy module in Bagpipes. The resulting resolution-matched stellar template is scaled by ~ 1.07 to account for the Kroupa-to-Chabrier IMF conversion between Bagpipes and CIGALE with negligible differences in the detailed spectral features. It is then combined with the featureless AGN continuum from CIGALE to form the continuum model used in spectra fitting, as shown in Extended Fig. 1. The center of the Balmer absorption line is tied to the narrow H α line, with its normalization fixed to the median value of the line-free region around H α . The narrow line centers are allowed to vary by $< 1 \text{ \AA}$ relative to the redshift reported by DJA. When multiple spectra with different instrument settings from various programs are available for the same object, we report the result with the highest ΔBIC .

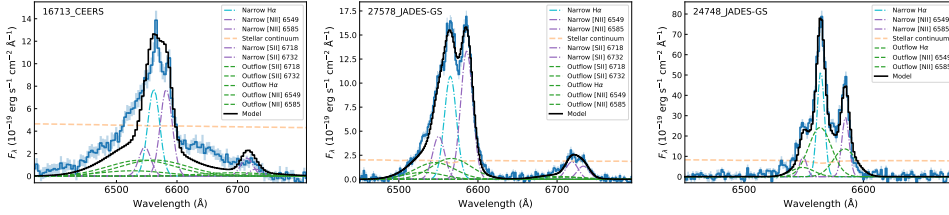
This spectral fitting procedure identifies 16 BLAGNs with $\text{SNR}(\text{H}\alpha_{\text{b}}) > 5$. We then visually inspected their spectral and SED fitting results, along with images, to select the final BLAGN sample for studying the $\mathcal{M}_{\text{BH}} - \mathcal{M}_{\star}$ relation. The total flux used to calibrate the prism spectrum of 13025-JADES-GS was contaminated by nearby companions not successfully deblended by ASTRODEEP. We recalibrated the spectrum using PSF-matched photometry within a $0.''5$ -diameter aperture, which captures most of the emission from the BLAGN, and repeated the SED fitting. The updated stellar mass is ~ 0.3 dex lower but remains consistent with a massive galaxy ($\log \mathcal{M}_{\star}/M_{\odot} \sim 10.34$). Additionally, we excluded two objects due to uncertain stellar mass estimates. Specifically, 106980-PRIMER-UDS exhibits a peculiar SED shape that cannot be fitted by our SED models, resulting in highly uncertain stellar mass estimates. 55620-PRIMER-UDS shows a characteristic V-shaped SED of little red dots [80]. The origin of this shape remains debated, with different interpretations (e.g., scattered AGN light or a combination of a blue galaxy and a reddened AGN) leading to orders of magnitude differences in the derived stellar mass [81]. Consequently, our final sample contains 14 BLAGNs hosted in “normal” massive galaxies, providing a lower limit of $\sim 27\%$ (14/52) for the fraction of BLAGNs in our massive galaxy sample.

Extended Fig. 2 presents the best-fit spectral decomposition results for these 14 BLAGNs. In addition to the broad and blueshifted outflow components detected in the [O III] spectra of 16713-CEERS, 27578-JADES-GS, and 24748-JADES-GS, which were included when fitting their H α and [N II] lines, a broad and symmetric BLR H α component is required to properly fit the residual emission both blueward of [N II] $\lambda 6549$ and redward of [N II] $\lambda 6585$ in all three objects. For comparison, the outflow-only model for these objects is displayed in Extended Fig. 3. The inclusion of the BLR H α component significantly improves the fit by $\Delta\text{BIC} > 200$ (Extended Table 2). For the remaining 11 objects, the outflow component is undetected in

[O III] or [S II] for 9 objects, supporting the BLR interpretation. For the other 2 objects (81571-PRIMER-UDS and 63546-JADES-GS), where [O III] and [S II] are not detected or covered, the BLR origin for broad H α is favored over outflows based on their lower BIC values.



Extended Fig. 2 Medium- and high-resolution spectra of the 14 BLAGNs identified in this work. The blue solid curve and shaded region represent the observed spectrum and flux uncertainty after subtracting the best-fit stellar continuum (orange dashed curve). The black solid curve represents the combined emission line model from a multi-component Gaussian fit. The purple dash-dotted curve represents the narrow [N II] and [S II] lines. The cyan and red dashed curves show the narrow and BLR H α lines. The green dashed curve displays the outflow component.



Extended Fig. 3 Outflow-only fitting results for 16713-CEERS, 27578-JADES-GS, and 24748-JADES-GS with a detected outflow component. The meaning of each component is the same as in Extended Fig. 2. In all cases, the outflow-only model produces poorer fits (BIC values higher by > 200) both blueward of [N II] $\lambda 6549$ and redward of [N II] $\lambda 6585$ compared to models that include the BLR H α component, as shown in Extended Fig. 2.

Black hole mass and bolometric luminosity of AGNs

The BH masses in AGNs can be determined by analyzing the motion of gas in the BLR, which is governed by the BH’s gravitational potential. Empirical relations were established between the width and luminosity of the broad line and the size and velocity of the BLR, enabling BH mass estimates using the so-called single-epoch virial estimator [28, 29]. Although the virial estimator is calibrated on a small sample of local reverberation mapped AGNs, and its applicability to the high-redshift universe is uncertain, it is the only consistent approach for measuring BH masses in our AGNs and other overmassive AGN samples in the literature.

In this work, we adopt the H α -based virial estimator from [31] to be consistent with most studies⁵:

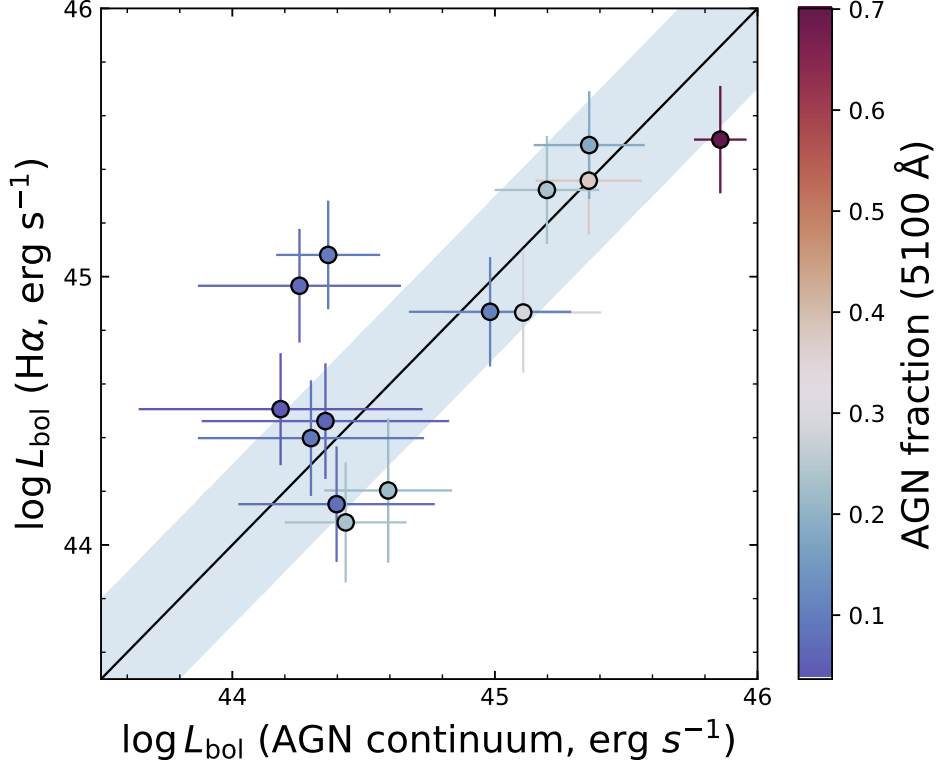
$$\log\left(\frac{\mathcal{M}_{\text{BH}}}{M_{\odot}}\right) = 6.57 + 0.47 \log\left(\frac{L_{\text{H}\alpha}}{10^{42} \text{ erg s}^{-1}}\right) + 2.06 \log\left(\frac{\text{FWHM}}{1000 \text{ km s}^{-1}}\right), \quad (1)$$

where $L_{\text{H}\alpha}$ and FWHM represent the luminosity and line width of the broad H α component, respectively. The H α luminosity is corrected for dust extinction using the A_V of the polar dust component derived by CIGALE. Our BLAGNs typically have $A_V \sim 0.5$ mag, consistent with that of LDs [3]. Since none of our BLAGNs are in the ABELL2744 field, no correction for the cluster magnification effect is needed. The intrinsic scatter of the H α -based BH mass estimator is ~ 0.35 dex [29]. The BH mass uncertainties are computed as the quadratic sum of the intrinsic scatter and the statistical uncertainty propagated from the line width and flux measurements in spectral fitting. An additional systematic uncertainty arises from the specific choice of the virial estimator, which is not included in the reported BH mass uncertainties. For reference, adopting the latest recipe from [82] and that from [32] results in even lower BH masses by ~ 0.17 and ~ 0.27 dex, respectively.

The AGN bolometric luminosity is derived from the correlation between the broad H α luminosity and the continuum luminosity at 5100 Å, following the relation in [32]

⁵The BH masses of literature AGN samples used in this work were recalibrated using the same broad H α based recipe adopted here, if a different one was used in the original paper.

and assuming a continuum bolometric conversion factor of 9.26 [83]. The $L_{\text{H}\alpha} - L_{5100}$ relation has an intrinsic scatter of ~ 0.2 dex, which is added in quadrature to the uncertainty in the derived L_{bol} . Additionally, L_{bol} can be directly estimated from the 5100 Å luminosity using the decomposed AGN continuum derived from CIGALE, corrected for extinction effects caused by polar dust. The comparison between the two measurements in Extended Fig. 4 demonstrates their consistency, with no systematic offset and within the scatter (~ 0.3 dex) observed for $\sim 24,000$ SDSS quasars at $z < 0.58$ that have H α coverage [84]. This consistency effectively validates our spectral and SED decomposition results, where the reddening from the polar dust is the only free parameter controlling the shape of the AGN continuum.



Extended Fig. 4 Comparison of AGN bolometric luminosities estimated from the decomposed AGN 5100 Å continuum luminosity in CIGALE and from the broad H α luminosity using the $L_{\text{H}\alpha} - L_{5100}$ relation in [32], assuming a continuum bolometric conversion factor of 9.26 [83]. Both luminosities are corrected for extinction using the A_V of the polar dust component. Each data point is color-coded by the AGN fraction at rest-frame 5100 Å. The solid black line and the blue shaded region represent the 1:1 relation and its ± 0.3 dex offset.

Extended Table 2 summarizes the derived SMBH and stellar properties of the 14 BLAGNs. Two objects were previously reported as BLAGNs in the literature.

[75] reported a BH mass of $\log \mathcal{M}_{\text{BH}}/M_{\odot} \sim 7.65$ for 70720-CEERS (named as RUBIES-UDS-58237 in their paper), which is in good agreement with our result ($\log \mathcal{M}_{\text{BH}}/M_{\odot} \sim 7.53$). Similarly, 7115-JADES-GN was studied in detail by [85], where the reported values of $\log \mathcal{M}_{\text{BH}}/M_{\odot} \sim 7.31$ and $\log \mathcal{M}_{\star}/M_{\odot} \sim 10.63$ are consistent with ours ($\log \mathcal{M}_{\text{BH}}/M_{\odot} \sim 7.61$, $\log \mathcal{M}_{\star}/M_{\odot} \sim 10.44$).

Physical properties of faint broad-line AGNs

The measured BH and stellar masses in Extended Table 2 show that, except for 16713-CEERS, the most luminous BLAGN identified in this work with $\mathcal{M}_{\text{BH}}/\mathcal{M}_{\star} \sim 10\%$, the remaining 13 faint BLAGNs have an average $\mathcal{M}_{\text{BH}}/\mathcal{M}_{\star}$ of $\sim 0.1\%$, consistent with the local value [7]. The decomposed stellar continuum for most faint AGNs (except 27578-JADES-GS) exhibits a characteristic shape typical of post-starburst galaxies and quiescent galaxies (Extended Fig. 1). As a sanity check, we verified that adding a recent burst or allowing abrupt quenching of recent star formation using the `sfhdelayedbq` module in CIGALE, or adding a nebular line model without masking emission lines in the fitting when generating the synthetic SEDs, has a negligible impact on the SED decomposition result and the derived stellar masses ($\Delta \mathcal{M}_{\star} \lesssim 0.1$ dex). Even with a burst component, the strong continuum emission blueward of the Balmer break in 7435-PRIMER-UDS is still primarily attributed to the AGN component in the CIGALE fitting, although there may be a low level of residual star formation. Therefore, the identification of normal and undermassive BHs and their declining SFH are robust against choices of SED models. The low $\mathcal{M}_{\text{BH}}/\mathcal{M}_{\star}$ ratio also holds for the eight most reliable BLAGNs with $\text{SNR}(\text{H}\alpha_{\text{b}}) > 10$ and $\Delta\text{BIC} > 20$ (Extended Table 2).

The bolometric luminosities and BH masses of our AGNs are comparable to those of LDs. However, as shown in Extended Table 2, our narrow $[\text{N II}] \lambda 6585/\text{H}\alpha$ ratios are ~ 25 times higher [3, 4], suggesting that these AGNs reside in massive, chemically enriched galaxies. The quenching nature of most objects and their high $[\text{N II}]/\text{H}\alpha$ ratio (~ 0.8 on average) further support the presence of AGNs, as the contribution from ongoing star formation to the emission lines is minimal, although the role of shock heating remains uncertain [3, 86]. These high-redshift analogs of local, chemically enriched AGNs with $\mathcal{M}_{\text{BH}}/\mathcal{M}_{\star} \sim 0.1\%$ represent the long-sought “normal” BH population in the distant Universe.

Acknowledgments. (Some of) The data products presented herein were retrieved from the Dawn JWST Archive (DJA). DJA is an initiative of the Cosmic Dawn Center (DAWN), which is funded by the Danish National Research Foundation under grant DNRF140.

Author Contributions

JL designed the program, led the data analysis, wrote the paper, and developed the main interpretation of the results. All authors contributed to the scientific interpretation of the results and presentation of the manuscript.

ID	redshift	$\log M_*$ (M_\odot)	$\log M_{\text{BH}}$ (M_\odot)	FWHM _b (km s^{-1})	ΔBIC	SNR($\text{H}\alpha_{\text{b}}$)	$\log L_{\text{bol}}(\text{cigale})$ (erg s^{-1})	$\log L_{\text{bol}}(\text{H}\alpha)$ (erg s^{-1})
70720-CEERS	3.651	10.81 ± 0.07	7.53 ± 0.36	2191 ± 141	42.60	20.9	44.26 ± 0.39	44.97 ± 0.21
7115-JADES-GN	4.128	10.44 ± 0.05	7.61 ± 0.40	3252 ± 673	51.20	8.8	44.35 ± 0.47	44.46 ± 0.22
13025-JADES-GS	3.472	10.34 ± 0.08	7.05 ± 0.44	2090 ± 596	21.70	8.7	44.59 ± 0.24	44.20 ± 0.27
16713-CEERS	3.666	10.01 ± 0.44	9.06 ± 0.35	9029 ± 389	575.40	33.9	45.86 ± 0.10	45.51 ± 0.20
19400-PRIMER-UDS	3.698	10.61 ± 0.08	8.03 ± 0.45	5371 ± 1644	27.60	6.9	44.30 ± 0.43	44.40 ± 0.22
7435-PRIMER-UDS	3.982	10.63 ± 0.12	7.31 ± 0.35	1419 ± 82	236.50	40.3	45.36 ± 0.20	45.36 ± 0.20
81571-PRIMER-UDS	3.942	10.56 ± 0.08	7.42 ± 0.35	1595 ± 64	108.20	31.1	45.20 ± 0.20	45.32 ± 0.20
247578-JADES-GS	3.704	10.22 ± 0.18	7.81 ± 0.37	3169 ± 368	333.80	26.7	45.11 ± 0.30	44.87 ± 0.22
24748-JADES-GS	3.704	10.83 ± 0.07	7.45 ± 0.35	1482 ± 74	202.50	46.4	45.36 ± 0.21	45.49 ± 0.20
70911-JADES-GS	3.672	11.19 ± 0.07	7.65 ± 0.36	2299 ± 159	103.90	15.5	44.37 ± 0.20	45.08 ± 0.20
24735-JADES-GS	3.584	10.33 ± 0.06	7.12 ± 0.39	2232 ± 406	21.90	7.7	44.40 ± 0.37	44.15 ± 0.22
32092-JADES-GS	3.473	10.07 ± 0.08	6.64 ± 0.42	1420 ± 371	14.90	5.7	44.43 ± 0.23	44.08 ± 0.22
63546-JADES-GS	3.605	10.68 ± 0.06	7.63 ± 0.40	3234 ± 664	52.50	14.3	44.18 ± 0.54	44.51 ± 0.21
35439-JADES-GN	3.127	10.92 ± 0.06	8.10 ± 0.37	4523 ± 577	99.40	10.2	44.98 ± 0.31	44.87 ± 0.20

ID	RA (deg)	DEC (deg)	$\log L_{\text{H}\alpha}$ (erg s^{-1})	$A_{\text{V,polar}}$ (mag)	[N II]/H α	program	grating
70720-CEERS	214.850569	52.866029	42.49 ± 0.08	0.52 ± 0.24	0.79	4233	g395m
7115-JADES-GN	189.265718	62.168393	41.91 ± 0.10	0.51 ± 0.24	1.46	1181	g395m
13025-JADES-GS	53.142828	-27.874048	41.54 ± 0.21	0.67 ± 0.19	0.58	1286	g395m
16713-CEERS	215.079264	52.934252	43.04 ± 0.02	0.70 ± 0.13	0.83	4233	g395m
19400-PRIMER-UDS	34.233628	-5.283850	41.84 ± 0.09	0.50 ± 0.25	0.56	4233	g395m
7435-PRIMER-UDS	34.363041	-5.306108	42.86 ± 0.02	0.71 ± 0.14	0.50	4233	g395m
81571-PRIMER-UDS	34.322542	-5.171391	42.86 ± 0.02	0.62 ± 0.18	0.97	1215	g395h
27578-JADES-GS	53.070272	-27.845596	42.38 ± 0.12	0.51 ± 0.23	1.26	1286	g395h
24748-JADES-GS	53.124445	-27.851707	43.06 ± 0.03	0.60 ± 0.20	0.75	1212	g395h
70911-JADES-GS	53.158329	-27.733605	42.66 ± 0.04	0.44 ± 0.25	0.44	1212	g395h
24735-JADES-GS	53.120018	-27.852026	41.58 ± 0.09	0.45 ± 0.27	0.53	1286	g235m
32092-JADES-GS	53.056726	-27.836383	41.42 ± 0.12	0.63 ± 0.18	0.49	1286	g235m
63546-JADES-GS	53.196909	-27.760532	41.96 ± 0.07	0.52 ± 0.24	2.35	1180	g235m
35439-JADES-GN	189.079806	62.244876	42.32 ± 0.05	0.65 ± 0.19	1.53	1211	g235h

Table 2 SMBH and galaxy properties for the 14 BLAGNs identified in this work. The source ID is named as the ASTRODEEP source ID combined with the field name. The BH mass, broad H α luminosity, and bolometric luminosity have been corrected for extinction using the polar dust extinction value $A_{\text{V,polar}}$.

Competing interests

The authors declare no competing interests.

Data availability

All the raw spectroscopic data are publicly available through the Mikulski Archive for Space Telescopes (MAST) under program ID 1180, 1181, 1199, 1210, 1211, 1212, 1213, 1214, 1215, 1286, 1345, 2198, 2561, 2565, 2750, 2756, 2767, 3073, 3215, 4233, 6541, 6585. The reduced NIRSspec spectroscopy and extracted HST and NIRCcam photometry that support the findings of this study are publicly available in the DJA archive (data release v3 as of Jan 8, 2025; <https://dawn-cph.github.io/dja/spectroscopy/nirspect/>) and the ASTRODEEP website (<http://www.astrodeep.eu/astrodeep-jwst-catalogs/>).

Code availability

The codes used to analyze data in this work are publicly available: CIGALE (<https://cigale.lam.fr/faq/>), msafit (<https://github.com/annadeg/jwst-msafit>), lmfit (<https://lmfit.github.io/lmfit-py/>), msaexp (<https://github.com/gbrammer/msaexp>)

Corresponding Author

Junyao Li (junyaoli@illinois.edu)

References

- [1] Kormendy, J., Ho, L.C.: Coevolution (Or Not) of Supermassive Black Holes and Host Galaxies. *ARA&A* **51**(1), 511–653 (2013) <https://doi.org/10.1146/annurev-astro-082708-101811> arXiv:1304.7762 [astro-ph.CO]
- [2] Schulze, A., Wisotzki, L.: Accounting for selection effects in the BH-bulge relations: no evidence for cosmological evolution. *MNRAS* **438**(4), 3422–3433 (2014) <https://doi.org/10.1093/mnras/stt2457> arXiv:1312.5610 [astro-ph.CO]
- [3] Maiolino, R., Scholtz, J., Curtis-Lake, E., Carniani, S., Baker, W., de Graaff, A., Tacchella, S., Übler, H., D’Eugenio, F., Witstok, J., Curti, M., Arribas, S., Bunker, A.J., Charlot, S., Chevallard, J., Eisenstein, D.J., Egami, E., Ji, Z., Jones, G.C., Lyu, J., Rawle, T., Robertson, B., Rujopakarn, W., Perna, M., Sun, F., Venturi, G., Williams, C.C., Willott, C.: JADES. The diverse population of infant Black Holes at $4 < z < 11$: merging, tiny, poor, but mighty. arXiv e-prints, 2308–01230 (2023) <https://doi.org/10.48550/arXiv.2308.01230> arXiv:2308.01230 [astro-ph.GA]
- [4] Harikane, Y., Zhang, Y., Nakajima, K., Ouchi, M., Isobe, Y., Ono, Y., Hatano, S., Xu, Y., Umeda, H.: A JWST/NIRSspec First Census of Broad-line AGNs at

- $z = 4-7$: Detection of 10 Faint AGNs with $M_{BH} 10^6-10^8 M_{\odot}$ and Their Host Galaxy Properties. *ApJ* **959**(1), 39 (2023) <https://doi.org/10.3847/1538-4357/ad029e> [arXiv:2303.11946](https://arxiv.org/abs/2303.11946) [astro-ph.GA]
- [5] Ding, X., Onoue, M., Silverman, J.D., Matsuoka, Y., Izumi, T., Strauss, M.A., Jahnke, K., Phillips, C.L., Li, J., Volonteri, M., Haiman, Z., Andika, I.T., Aoki, K., Baba, S., Bieri, R., Bosman, S.E.I., Bottrell, C., Eilers, A.-C., Fujimoto, S., Habouzit, M., Imanishi, M., Inayoshi, K., Iwasawa, K., Kashikawa, N., Kawaguchi, T., Kohno, K., Lee, C.-H., Lupi, A., Lyu, J., Nagao, T., Overzier, R., Schindler, J.-T., Schramm, M., Shimasaku, K., Toba, Y., Trakhtenbrot, B., Trebitsch, M., Treu, T., Umehata, H., Venemans, B.P., Vestergaard, M., Walter, F., Wang, F., Yang, J.: Detection of stellar light from quasar host galaxies at redshifts above 6. *Nature* **621**(7977), 51–55 (2023) <https://doi.org/10.1038/s41586-023-06345-5> [arXiv:2211.14329](https://arxiv.org/abs/2211.14329) [astro-ph.GA]
- [6] Li, J., Silverman, J.D., Shen, Y., Volonteri, M., Jahnke, K., Zhuang, M.-Y., Scoggins, M.T., Ding, X., Harikane, Y., Onoue, M., Tanaka, T.S.: Tip of the iceberg: overmassive black holes at $z \gtrsim 7$ found by JWST are not inconsistent with the local $M_{BH}-M_{*}$ relation. *arXiv e-prints*, 2403–00074 (2024) <https://doi.org/10.48550/arXiv.2403.00074> [arXiv:2403.00074](https://arxiv.org/abs/2403.00074) [astro-ph.GA]
- [7] Greene, J.E., Strader, J., Ho, L.C.: Intermediate-Mass Black Holes. *ARA&A* **58**, 257–312 (2020) <https://doi.org/10.1146/annurev-astro-032620-021835> [arXiv:1911.09678](https://arxiv.org/abs/1911.09678) [astro-ph.GA]
- [8] Dattathri, S., Natarajan, P., Porras-Valverde, A.J., Burke, C.J., Chen, N., Di Matteo, T., Ni, Y.: The redshift evolution of the $M_{BH} - M_{*}$ scaling relation: new insights from cosmological simulations and semi-analytic models. *arXiv e-prints*, 2410–13958 (2024) <https://doi.org/10.48550/arXiv.2410.13958> [arXiv:2410.13958](https://arxiv.org/abs/2410.13958) [astro-ph.GA]
- [9] Weller, E.J., Pacucci, F., Ni, Y., Hernquist, L., Park, M.: Discrepancies Between JWST Observations and Simulations of Quenched Massive Galaxies at $z > 3$: A Comparative Study With IllustrisTNG and ASTRID. *arXiv e-prints*, 2406–02664 (2024) <https://doi.org/10.48550/arXiv.2406.02664> [arXiv:2406.02664](https://arxiv.org/abs/2406.02664) [astro-ph.GA]
- [10] Pacucci, F., Loeb, A.: The Redshift Evolution of the $M - M_{*}$ Relation for JWST’s Supermassive Black Holes at $z \gtrsim 4$. *ApJ* **964**(2), 154 (2024) <https://doi.org/10.3847/1538-4357/ad3044> [arXiv:2401.04159](https://arxiv.org/abs/2401.04159) [astro-ph.GA]
- [11] Volonteri, M.: Formation of supermassive black holes. *A&A Rev.* **18**(3), 279–315 (2010) <https://doi.org/10.1007/s00159-010-0029-x> [arXiv:1003.4404](https://arxiv.org/abs/1003.4404) [astro-ph.CO]
- [12] King, A., Pounds, K.: Powerful Outflows and Feedback from Active Galactic Nuclei. *ARA&A* **53**, 115–154 (2015) <https://doi.org/10.1146/>

- [13] Peng, C.Y.: How Mergers May Affect the Mass Scaling Relation between Gravitationally Bound Systems. *ApJ* **671**(2), 1098–1107 (2007) <https://doi.org/10.1086/522774> arXiv:0704.1860 [astro-ph]
- [14] Jahnke, K., Macciò, A.V.: The Non-causal Origin of the Black-hole-galaxy Scaling Relations. *ApJ* **734**(2), 92 (2011) <https://doi.org/10.1088/0004-637X/734/2/92> arXiv:1006.0482 [astro-ph.CO]
- [15] Habouzit, M., Li, Y., Somerville, R.S., Genel, S., Pillepich, A., Volonteri, M., Davé, R., Rosas-Guevara, Y., McAlpine, S., Peirani, S., Hernquist, L., Anglés-Alcázar, D., Reines, A., Bower, R., Dubois, Y., Nelson, D., Pichon, C., Vogelsberger, M.: Supermassive black holes in cosmological simulations I: M_{BH} - M_* relation and black hole mass function. *MNRAS* **503**(2), 1940–1975 (2021) <https://doi.org/10.1093/mnras/stab496> arXiv:2006.10094 [astro-ph.GA]
- [16] Li, J., Silverman, J.D., Ding, X., Strauss, M.A., Goulding, A., Schramm, M., Yesuf, H.M., Sun, M., Xue, Y., Birrer, S., Shi, J., Toba, Y., Nagao, T., Imanishi, M.: Synchronized Coevolution between Supermassive Black Holes and Galaxies over the Last Seven Billion Years as Revealed by Hyper Suprime-Cam. *ApJ* **922**(2), 142 (2021) <https://doi.org/10.3847/1538-4357/ac2301> arXiv:2109.02751 [astro-ph.GA]
- [17] Ding, X., Silverman, J.D., Treu, T., Li, J., Bhowmick, A.K., Menci, N., Volonteri, M., Blecha, L., Di Matteo, T., Dubois, Y.: Concordance between Observations and Simulations in the Evolution of the Mass Relation between Supermassive Black Holes and Their Host Galaxies. *ApJ* **933**(2), 132 (2022) <https://doi.org/10.3847/1538-4357/ac714c> arXiv:2205.04481 [astro-ph.GA]
- [18] Zhuang, M.-Y., Ho, L.C.: Evolutionary paths of active galactic nuclei and their host galaxies. *Nature Astronomy* **7**, 1376–1389 (2023) <https://doi.org/10.1038/s41550-023-02051-4> arXiv:2308.08603 [astro-ph.GA]
- [19] Tanaka, T.S., Silverman, J.D., Ding, X., Jahnke, K., Trakhtenbrot, B., Lambrides, E., Onoue, M., Taufik Andika, I., Bongiorno, A., Faisst, A.L., Gillman, S., Hayward, C.C., Hirschmann, M., Koekemoer, A., Kokorev, V., Liu, Z., Magdis, G.E., Renzini, A., Casey, C., Drakos, N.E., Franco, M., Gozaliasl, G., Kartaltepe, J., Liu, D., McCracken, H.J., Rhodes, J., Robertson, B., Toft, S.: The $M_{BH} - M_*$ relation up to $z \sim 2$ through decomposition of COSMOS-Web NIRCcam images. arXiv e-prints, 2401–13742 (2024) <https://doi.org/10.48550/arXiv.2401.13742> arXiv:2401.13742 [astro-ph.GA]
- [20] Bhowmick, A.K., Blecha, L., Torrey, P., Kelley, L.Z., Weinberger, R., Vogelsberger, M., Hernquist, L., Somerville, R.S., Evans, A.E.: Introducing the BRAHMA simulation suite: signatures of low-mass black hole seeding models in cosmological simulations. *MNRAS* **531**(4), 4311–4335 (2024) <https://doi.org/10.1093/mnras/stae1000>

- [21] Matthee, J., Naidu, R.P., Brammer, G., Chisholm, J., Eilers, A.-C., Goulding, A., Greene, J., Kashino, D., Labbe, I., Lilly, S.J., Mackenzie, R., Oesch, P.A., Weibel, A., Wuyts, S., Xiao, M., Bordoloi, R., Bouwens, R., van Dokkum, P., Illingworth, G., Kramarenko, I., Maseda, M.V., Mason, C., Meyer, R.A., Nelson, E.J., Reddy, N.A., Shivaiei, I., Simcoe, R.A., Yue, M.: Little Red Dots: An Abundant Population of Faint Active Galactic Nuclei at $z \sim 5$ Revealed by the EIGER and FRESCO JWST Surveys. *ApJ* **963**(2), 129 (2024) <https://doi.org/10.3847/1538-4357/ad2345> arXiv:2306.05448 [astro-ph.GA]
- [22] Stone, M.A., Lyu, J., Rieke, G.H., Alberts, S., Hainline, K.N.: Undermassive Host Galaxies of Five $z \sim 6$ Luminous Quasars Detected with JWST. *ApJ* **964**(1), 90 (2024) <https://doi.org/10.3847/1538-4357/ad2a57> arXiv:2310.18395 [astro-ph.GA]
- [23] Yue, M., Eilers, A.-C., Simcoe, R.A., Mackenzie, R., Matthee, J., Kashino, D., Bordoloi, R., Lilly, S.J., Naidu, R.P.: EIGER. V. Characterizing the Host Galaxies of Luminous Quasars at $z \gtrsim 6$. *ApJ* **966**(2), 176 (2024) <https://doi.org/10.3847/1538-4357/ad3914> arXiv:2309.04614 [astro-ph.GA]
- [24] Natarajan, P., Pacucci, F., Ricarte, A., Bogdán, Á., Goulding, A.D., Cappelluti, N.: First Detection of an Overmassive Black Hole Galaxy UHZ1: Evidence for Heavy Black Hole Seed Formation from Direct Collapse. *ApJ* **960**(1), 1 (2024) <https://doi.org/10.3847/2041-8213/ad0e76> arXiv:2308.02654 [astro-ph.HE]
- [25] Lauer, T.R., Tremaine, S., Richstone, D., Faber, S.M.: Selection Bias in Observing the Cosmological Evolution of the M - σ and M - L Relationships. *ApJ* **670**(1), 249–260 (2007) <https://doi.org/10.1086/522083> arXiv:0705.4103 [astro-ph]
- [26] Volonteri, M., Habouzit, M., Colpi, M.: What if young $z \lesssim 9$ JWST galaxies hosted massive black holes? *MNRAS* **521**(1), 241–250 (2023) <https://doi.org/10.1093/mnras/stad499> arXiv:2212.04710 [astro-ph.GA]
- [27] Fan, X., Bañados, E., Simcoe, R.A.: Quasars and the Intergalactic Medium at Cosmic Dawn. *ARA&A* **61**, 373–426 (2023) <https://doi.org/10.1146/annurev-astro-052920-102455> arXiv:2212.06907 [astro-ph.GA]
- [28] Vestergaard, M., Peterson, B.M.: Determining Central Black Hole Masses in Distant Active Galaxies and Quasars. II. Improved Optical and UV Scaling Relationships. *ApJ* **641**(2), 689–709 (2006) <https://doi.org/10.1086/500572> arXiv:astro-ph/0601303 [astro-ph]
- [29] Shen, Y., Grier, C.J., Horne, K., Stone, Z., Li, J.I., Yang, Q., Homayouni, Y., Trump, J.R., Anderson, S.F., Brandt, W.N., Hall, P.B., Ho, L.C., Jiang, L., Petitjean, P., Schneider, D.P., Tao, C., Donnan, F.R., AlSayyad, Y., Bershad, M.A., Blanton, M.R., Bizyaev, D., Bundy, K., Chen, Y., Davis, M.C., Dawson, K.,

- Fan, X., Greene, J.E., Gröller, H., Guo, Y., Ibarra-Medel, H., Jiang, Y., Keenan, R.P., Kollmeier, J.A., Lejoly, C., Li, Z., de la Macorra, A., Moe, M., Nie, J., Rossi, G., Smith, P.S., Tee, W.L., Weijmans, A.-M., Xu, J., Yue, M., Zhou, X., Zhou, Z., Zou, H.: The Sloan Digital Sky Survey Reverberation Mapping Project: Key Results. *ApJS* **272**(2), 26 (2024) <https://doi.org/10.3847/1538-4365/ad3936> [arXiv:2305.01014](https://arxiv.org/abs/2305.01014) [astro-ph.GA]
- [30] Merlin, E., Santini, P., Paris, D., Castellano, M., Fontana, A., Treu, T., Finkelstein, S.L., Dunlop, J.S., Arrabal Haro, P., Bagley, M., Boyett, K., Calabrò, A., Correnti, M., Davis, K., Dickinson, M., Donnan, C.T., Ferguson, H.C., Fortuni, F., Giavalisco, M., Glazebrook, K., Grazian, A., Grogin, N.A., Hathi, N., Hirschmann, M., Kartaltepe, J.S., Kewley, L.J., Kirkpatrick, A., Kocevski, D.D., Koekemoer, A.M., Leung, G., Lotz, J.M., Magee, D.K., Marchesini, D., Mascia, S., McLeod, D.J., McLure, R.J., Nanayakkara, T., Napolitano, L., Nonino, M., Papovich, C., Pentericci, L., Pérez-González, P.G., Pirzkal, N., Ravindranath, S., Roberts-Borsani, G., Somerville, R.S., Trenti, M., Trump, J.R., Vulcani, B., Wang, X., Watson, P.J., Wilkins, S.M., Yang, G., Yung, L.Y.A.: ASTRODEEP-JWST: NIRCам-HST multiband photometry and redshifts for half a million sources in six extragalactic deep fields. arXiv e-prints, 2409–00169 (2024) <https://doi.org/10.48550/arXiv.2409.00169> [arXiv:2409.00169](https://arxiv.org/abs/2409.00169) [astro-ph.GA]
- [31] Reines, A.E., Volonteri, M.: Relations between Central Black Hole Mass and Total Galaxy Stellar Mass in the Local Universe. *ApJ* **813**(2), 82 (2015) <https://doi.org/10.1088/0004-637X/813/2/82> [arXiv:1508.06274](https://arxiv.org/abs/1508.06274) [astro-ph.GA]
- [32] Greene, J.E., Ho, L.C.: Estimating Black Hole Masses in Active Galaxies Using the H α Emission Line. *ApJ* **630**(1), 122–129 (2005) <https://doi.org/10.1086/431897> [arXiv:astro-ph/0508335](https://arxiv.org/abs/astro-ph/0508335) [astro-ph]
- [33] Carnall, A.C., McLeod, D.J., McLure, R.J., Dunlop, J.S., Begley, R., Cullen, F., Donnan, C.T., Hamadouche, M.L., Jewell, S.M., Jones, E.W., Pollock, C.L., Wild, V.: A surprising abundance of massive quiescent galaxies at $3 < z < 5$ in the first data from JWST CEERS. *MNRAS* **520**(3), 3974–3985 (2023) <https://doi.org/10.1093/mnras/stad369> [arXiv:2208.00986](https://arxiv.org/abs/2208.00986) [astro-ph.GA]
- [34] Nanayakkara, T., Glazebrook, K., Jacobs, C., Kawinwanichakij, L., Schreiber, C., Brammer, G., Esdaile, J., Kacprzak, G.G., Labbe, I., Lagos, C., Marchesini, D., Marsan, Z.C., Oesch, P.A., Papovich, C., Remus, R.-S., Tran, K.-V.H.: A population of faint, old, and massive quiescent galaxies at $3 < z < 4$ revealed by JWST NIRSpec Spectroscopy. *Scientific Reports* **14**, 3724 (2024) <https://doi.org/10.1038/s41598-024-52585-4> [arXiv:2212.11638](https://arxiv.org/abs/2212.11638) [astro-ph.GA]
- [35] Park, M., Belli, S., Conroy, C., Johnson, B.D., Davies, R.L., Leja, J., Tacchella, S., Mendel, J.T., Benton, C., Bugiani, L., Emami, R., Khoram, A.H., Li, Y., Maheson, G., Mathews, E.P., Naidu, R.P., Nelson, E.J., Terrazas, B.A., Weinberger, R.: Widespread Rapid Quenching at Cosmic Noon Revealed by JWST Deep

Spectroscopy. *ApJ* **976**(1), 72 (2024) <https://doi.org/10.3847/1538-4357/ad7e15>
[arXiv:2404.17945](https://arxiv.org/abs/2404.17945) [astro-ph.GA]

- [36] Baker, W.M., Lim, S., D'Eugenio, F., Maiolino, R., Ji, Z., Arribas, S., Bunker, A.J., Carniani, S., Charlot, S., de Graaff, A., Hainline, K., Looser, T.J., Lyu, J., Rinaldi, P., Robertson, B., Schaller, M., Schaye, J., Scholtz, J., Ubler, H., Williams, C.C., Willmer, C.N.A., Willott, C., Zhu, Y.: The abundance and nature of high-redshift quiescent galaxies from JADES spectroscopy and the FLAMINGO simulations. *arXiv e-prints*, 2410–14773 (2024) <https://doi.org/10.48550/arXiv.2410.14773> [arXiv:2410.14773](https://arxiv.org/abs/2410.14773) [astro-ph.GA]
- [37] de Graaff, A., Brammer, G., Weibel, A., Lewis, Z., Maseda, M.V., Oesch, P.A., Bezanson, R., Boogaard, L.A., Cleri, N.J., Cooper, O.R., Gottumukkala, R., Greene, J.E., Hirschmann, M., Hviding, R.E., Katz, H., Labbé, I., Leja, J., Matthee, J., McConachie, I., Miller, T.B., Naidu, R.P., Price, S.H., Rix, H.-W., Setton, D.J., Suess, K.A., Wang, B., Whitaker, K.E., Williams, C.C.: RUBIES: a complete census of the bright and red distant Universe with JWST/NIRSpec. *arXiv e-prints*, 2409–05948 (2024) <https://doi.org/10.48550/arXiv.2409.05948> [arXiv:2409.05948](https://arxiv.org/abs/2409.05948) [astro-ph.GA]
- [38] D'Eugenio, F., Perez-Gonzalez, P., Maiolino, R., Scholtz, J., Perna, M., Circosta, C., Uebler, H., Arribas, S., Boeker, T., Bunker, A., Carniani, S., Charlot, S., Chevallard, J., Cresci, G., Curtis-Lake, E., Jones, G., Kumari, N., Lamperti, I., Looser, T., Parlanti, E., Rix, H.-W., Robertson, B., Rodriguez Del Pino, B., Tacchella, S., Venturi, G., Willott, C.: A fast-rotator post-starburst galaxy quenched by supermassive black-hole feedback at $z=3$. *arXiv e-prints*, 2308–06317 (2023) <https://doi.org/10.48550/arXiv.2308.06317> [arXiv:2308.06317](https://arxiv.org/abs/2308.06317) [astro-ph.GA]
- [39] Boyett, K., Bunker, A.J., Curtis-Lake, E., Chevallard, J., Cameron, A.J., Jones, G.C., Saxena, A., Charlot, S., Curti, M., Wallace, I.E.B., Arribas, S., Carniani, S., Willott, C., Alberts, S., Eisenstein, D.J., Hainline, K., Hausen, R., Johnson, B.D., Rieke, M., Robertson, B., Stark, D.P., Tacchella, S., Williams, C.C., Chen, Z., Egami, E., Endsley, R., Kumari, N., Laseter, I., Looser, T.J., Maseda, M.V., Scholtz, J., Shivaee, I., Simmonds, C., Smit, R., Übler, H., Witstok, J.: Extreme emission line galaxies detected in JADES JWST/NIRSpec - I. Inferred galaxy properties. *MNRAS* **535**(2), 1796–1828 (2024) <https://doi.org/10.1093/mnras/stae2430> [arXiv:2401.16934](https://arxiv.org/abs/2401.16934) [astro-ph.GA]
- [40] Giménez-Arteaga, C., Oesch, P.A., Brammer, G.B., Valentino, F., Mason, C.A., Weibel, A., Barrufet, L., Fujimoto, S., Heintz, K.E., Nelson, E.J., Strait, V.B., Suess, K.A., Gibson, J.: Spatially Resolved Properties of Galaxies at $5 < z < 9$ in the SMACS 0723 JWST ERO Field. *ApJ* **948**(2), 126 (2023) <https://doi.org/10.3847/1538-4357/acc5ea> [arXiv:2212.08670](https://arxiv.org/abs/2212.08670) [astro-ph.GA]
- [41] Giménez-Arteaga, C., Fujimoto, S., Valentino, F., Brammer, G.B., Mason, C.A., Rizzo, F., Rusakov, V., Colina, L., Prieto-Lyon, G., Oesch, P.A., Espada, D.,

- Heintz, K.E., Knudsen, K.K., Dessauges-Zavadsky, M., Laporte, N., Lee, M., Magdis, G.E., Ono, Y., Ao, Y., Ouchi, M., Kohno, K., Koekemoer, A.M.: Outshining in the Spatially Resolved Analysis of a Strongly-Lensed Galaxy at $z=6.072$ with JWST NIRCam. arXiv e-prints, 2402–17875 (2024) [arXiv:2402.17875](https://arxiv.org/abs/2402.17875) [astro-ph.GA]
- [42] Onoue, M., Ding, X., Silverman, J.D., Matsuoka, Y., Izumi, T., Strauss, M.A., Ward, C., Phillips, C.L., Andika, I.T., Aoki, K., Arita, J., Baba, S., Bieri, R., Bosman, S.E.I., Eilers, A.-C., Fujimoto, S., Habouzit, M., Haiman, Z., Imanishi, M., Inayoshi, K., Ito, K., Iwasawa, K., Jahnke, K., Kashikawa, N., Kawaguchi, T., Kohno, K., Lee, C.-H., Li, J., Lupi, A., Lyu, J., Nagao, T., Overzier, R., Schindler, J.-T., Schramm, M., Scoggins, M.T., Shimasaku, K., Toba, Y., Trakhtenbrot, B., Trebitsch, M., Treu, T., Umehata, H., Venemans, B., Vestergaard, M., Volonteri, M., Walter, F., Wang, F., Yang, J., Zhang, H.: A Post-Starburst Pathway to Forming Massive Galaxies and Their Black Holes at $z \gtrsim 6$. arXiv e-prints, 2409–07113 (2024) <https://doi.org/10.48550/arXiv.2409.07113> [arXiv:2409.07113](https://arxiv.org/abs/2409.07113) [astro-ph.GA]
- [43] Baggen, J.F.W., van Dokkum, P., Labbé, I., Brammer, G., Miller, T.B., Bezanson, R., Leja, J., Wang, B., Whitaker, K.E., Suess, K.A., Nelson, E.J.: Sizes and Mass Profiles of Candidate Massive Galaxies Discovered by JWST at $7 \lesssim z \lesssim 9$: Evidence for Very Early Formation of the Central 100 pc of Present-day Ellipticals. *ApJ* **955**(1), 12 (2023) <https://doi.org/10.3847/2041-8213/acf5ef> [arXiv:2305.17162](https://arxiv.org/abs/2305.17162) [astro-ph.GA]
- [44] Habouzit, M., Volonteri, M., Dubois, Y.: Blossoms from black hole seeds: properties and early growth regulated by supernova feedback. *MNRAS* **468**(4), 3935–3948 (2017) <https://doi.org/10.1093/mnras/stx666> [arXiv:1605.09394](https://arxiv.org/abs/1605.09394) [astro-ph.GA]
- [45] Zhu, Q., Li, Y., Li, Y., Maji, M., Yajima, H., Schneider, R., Hernquist, L.: The formation of the first quasars: the black hole seeds, accretion, and feedback models. *MNRAS* **514**(4), 5583–5606 (2022) <https://doi.org/10.1093/mnras/stac1556> [arXiv:2012.01458](https://arxiv.org/abs/2012.01458) [astro-ph.GA]
- [46] Ni, Y., Chen, N., Zhou, Y., Park, M., Yang, Y., DiMatteo, T., Bird, S., Croft, R.: The Astrid Simulation: Evolution of black holes and galaxies to $z=0.5$ and different evolution pathways for galaxy quenching. arXiv e-prints, 2409–10666 (2024) <https://doi.org/10.48550/arXiv.2409.10666> [arXiv:2409.10666](https://arxiv.org/abs/2409.10666) [astro-ph.GA]
- [47] Shen, Y., Zhuang, M.-Y., Li, J., Burgasser, A.J., Fan, X., Greene, J.E., Narayan, G., Shapley, A.E., Sun, F., Wang, F., Yang, Q.: NEXUS: the North ecliptic pole EXtragalactic Unified Survey. arXiv e-prints, 2408–12713 (2024) <https://doi.org/10.48550/arXiv.2408.12713> [arXiv:2408.12713](https://arxiv.org/abs/2408.12713) [astro-ph.GA]
- [48] de Graaff, A., Setton, D.J., Brammer, G., Cutler, S., Suess, K.A., Labbé, I., Leja, J., Weibel, A., Maseda, M.V., Whitaker, K.E., Bezanson, R., Boogaard, L.A.,

- Cleri, N.J., De Lucia, G., Franx, M., Greene, J.E., Hirschmann, M., Matthee, J., McConachie, I., Naidu, R.P., Oesch, P.A., Price, S.H., Rix, H.-W., Valentino, F., Wang, B., Williams, C.C.: Efficient formation of a massive quiescent galaxy at redshift 4.9. *Nature Astronomy* (2024) <https://doi.org/10.1038/s41550-024-02424-3> [arXiv:2404.05683](https://arxiv.org/abs/2404.05683) [astro-ph.GA]
- [49] Deng, Y., Li, H., Liu, B., Kannan, R., Smith, A., Bryan, G.L.: RIGEL: Simulating dwarf galaxies at solar mass resolution with radiative transfer and feedback from individual massive stars. *A&A* **691**, 231 (2024) <https://doi.org/10.1051/0004-6361/202450699> [arXiv:2405.08869](https://arxiv.org/abs/2405.08869) [astro-ph.GA]
- [50] Aird, J., Coil, A.L., Kocevski, D.D.: AGN accretion and black hole growth across compact and extended galaxy evolution phases. *MNRAS* **515**(4), 4860–4889 (2022) <https://doi.org/10.1093/mnras/stac2103> [arXiv:2201.11756](https://arxiv.org/abs/2201.11756) [astro-ph.GA]
- [51] Chabrier, G.: Galactic Stellar and Substellar Initial Mass Function. *PASP* **115**(809), 763–795 (2003) <https://doi.org/10.1086/376392> [arXiv:astro-ph/0304382](https://arxiv.org/abs/astro-ph/0304382) [astro-ph]
- [52] Brammer, G.: msaexp: NIRSpec Analysis Tools. <https://doi.org/10.5281/zenodo.7299500>
- [53] Heintz, K.E., Watson, D., Brammer, G., Vejlgaard, S., Hutter, A., Strait, V.B., Matthee, J., Oesch, P.A., Jakobsson, P., Tanvir, N.R., Laursen, P., Naidu, R.P., Mason, C.A., Killi, M., Jung, I., Hsiao, T.Y.-Y., Abdurro’uf, Coe, D., Arrabal Haro, P., Finkelstein, S.L., Toft, S.: Strong damped Lyman- α absorption in young star-forming galaxies at redshifts 9 to 11. *Science* **384**(6698), 890–894 (2024) <https://doi.org/10.1126/science.adj0343> [arXiv:2306.00647](https://arxiv.org/abs/2306.00647) [astro-ph.GA]
- [54] Horne, K.: An optimal extraction algorithm for CCD spectroscopy. *PASP* **98**, 609–617 (1986) <https://doi.org/10.1086/131801>
- [55] Merlin, E., Bonchi, A., Paris, D., Belfiori, D., Fontana, A., Castellano, M., Nonino, M., Polenta, G., Santini, P., Yang, L., Glazebrook, K., Treu, T., Roberts-Borsani, G., Trenti, M., Birrer, S., Brammer, G., Grillo, C., Calabrò, A., Marchesini, D., Mason, C., Mercurio, A., Morishita, T., Strait, V., Boyett, K., Leethochawalit, N., Nanayakkara, T., Vulcani, B., Bradac, M., Wang, X.: Early Results from GLASS-JWST. II. NIRCcam Extragalactic Imaging and Photometric Catalog. *ApJ* **938**(2), 14 (2022) <https://doi.org/10.3847/2041-8213/ac8f93> [arXiv:2207.11701](https://arxiv.org/abs/2207.11701) [astro-ph.GA]
- [56] Wang, T., Sun, H., Zhou, L., Xu, K., Cheng, C., Li, Z., Chen, Y., Mo, H.J., Dekel, A., Yang, T., Wang, Y., Zheng, X., Cai, Z., Elbaz, D., Dai, Y.-S., Huang, J.-S.: MASSive galaxies aCROSS cOSmic time revealed by JWST/MIRI (MACROSS): The true number density of massive galaxies in the early Universe. *arXiv e-prints*, 2403–02399 (2024) <https://doi.org/10.48550/arXiv.2403.02399> [arXiv:2403.02399](https://arxiv.org/abs/2403.02399) [astro-ph.GA]

- [57] Eisenstein, D.J., Willott, C., Alberts, S., Arribas, S., Bonaventura, N., Bunker, A.J., Cameron, A.J., Carniani, S., Charlot, S., Curtis-Lake, E., D'Eugenio, F., Endsley, R., Ferruit, P., Giardino, G., Hainline, K., Hausen, R., Jakobsen, P., Johnson, B.D., Maiolino, R., Rieke, M., Rieke, G., Rix, H.-W., Robertson, B., Stark, D.P., Tacchella, S., Williams, C.C., Willmer, C.N.A., Baker, W.M., Baum, S., Bhatawdekar, R., Boyett, K., Chen, Z., Chevallard, J., Circosta, C., Curti, M., Danhaive, A.L., DeCoursey, C., de Graaff, A., Dressler, A., Egami, E., Helton, J.M., Hviding, R.E., Ji, Z., Jones, G.C., Kumari, N., Lützgendorf, N., Laseter, I., Looser, T.J., Lyu, J., Maseda, M.V., Nelson, E., Parlanti, E., Perna, M., Puskás, D., Rawle, T., Rodríguez Del Pino, B., Sandles, L., Saxena, A., Scholtz, J., Sharpe, K., Shivaiei, I., Silcock, M.S., Simmonds, C., Skarbinski, M., Smit, R., Stone, M., Suess, K.A., Sun, F., Tang, M., Topping, M.W., Übler, H., Villanueva, N.C., Wallace, I.E.B., Whitler, L., Witstok, J., Woodrum, C.: Overview of the JWST Advanced Deep Extragalactic Survey (JADES). arXiv e-prints, 2306–02465 (2023) <https://doi.org/10.48550/arXiv.2306.02465> arXiv:2306.02465 [astro-ph.GA]
- [58] Stiavelli, M., Morishita, T., Chiaberge, M., Grillo, C., Leethochawalit, N., Rosati, P., Schuldt, S., Trenti, M., Treu, T.: The Puzzling Properties of the MACS1149-JD1 Galaxy at $z = 9.11$. *ApJ* **957**(2), 18 (2023) <https://doi.org/10.3847/2041-8213/ad0159> arXiv:2308.14696 [astro-ph.GA]
- [59] Maseda, M.V., de Graaff, A., Franx, M., Rix, H.-W., Carniani, S., Laseter, I., Dudzevičiūtė, U., Rawle, T., Parlanti, E., Arribas, S., Bunker, A.J., Cameron, A.J., Charlot, S., Curti, M., D'Eugenio, F., Jones, G.C., Kumari, N., Maiolino, R., Übler, H., Saxena, A., Smit, R., Willott, C., Witstok, J.: The NIRSpec Wide GTO Survey. *A&A* **689**, 73 (2024) <https://doi.org/10.1051/0004-6361/202449914> arXiv:2403.05506 [astro-ph.GA]
- [60] Finkelstein, S.L., Bagley, M.B., Arrabal Haro, P., Dickinson, M., Ferguson, H.C., Kartaltepe, J.S., Kocevski, D.D., Koekemoer, A.M., Lotz, J.M., Papovich, C., Perez-Gonzalez, P.G., Pirzkal, N., Somerville, R.S., Trump, J.R., Yang, G., Yung, L.Y.A., Fontana, A., Grazian, A., Grogin, N.A., Kewley, L.J., Kirkpatrick, A., Larson, R.L., Pentericci, L., Ravindranath, S., Wilkins, S.M., Almaini, O., Amorin, R.O., Barro, G., Bhatawdekar, R., Bisigello, L., Brooks, M., Buitrago, F., Calabro, A., Castellano, M., Cheng, Y., Cleri, N.J., Cole, J.W., Cooper, M.C., Cooper, O.R., Costantin, L., Cox, I.G., Croton, D., Daddi, E., Davis, K., Dekel, A., Elbaz, D., Fernandez, V., Fujimoto, S., Gandolfi, G., Gardner, J.P., Gawiser, E., Giavalisco, M., Gomez-Guijarro, C., Guo, Y., Gupta, A.R., Hathi, N.P., Harish, S., Henry, A., Hirschmann, M., Hu, W., Hutchison, T.A., Iyer, K.G., Jaskot, A.E., Jha, S.W., Jung, I., Kokorev, V., Kurczynski, P., Leung, G.C.K., Llerena, M., Long, A.S., Lucas, R.A., Lu, S., McGrath, E.J., McIntosh, D.H., Merlin, E., Morales, A.M., Napolitano, L., Pacucci, F., Pandya, V., Rafelski, M., Rodighiero, G., Rose, C., Santini, P., Seille, L.-M., Simons, R.C., Shen, L., Straughn, A.N., Tacchella, S., Vanderhoof, B.N., Vega-Ferrero, J., Weiner, B.J., Willmer, C.N.A., Zhu, P., Bell, E.F., Wuyts, S., Holwerda, B.W., Wang, X., Wang, W., Zavala, J.A.:

The Cosmic Evolution Early Release Science Survey (CEERS). arXiv e-prints, 2501–04085 (2025) <https://doi.org/10.48550/arXiv.2501.04085> arXiv:2501.04085 [astro-ph.GA]

- [61] Barrufet, L., Oesch, P.A., Marques-Chaves, R., Arellano-Cordova, K., Baggen, J.F.W., Carnall, A.C., Cullen, F., Dunlop, J.S., Gottumukkala, R., Fudamoto, Y., Illingworth, G.D., Magee, D., McLure, R.J., McLeod, D.J., Michałowski, M.J., Stefanon, M., van Dokkum, P.G., Weibel, A.: Quiescent or dusty? Unveiling the nature of extremely red galaxies at $z \gtrsim 3$. MNRAS (2025) <https://doi.org/10.1093/mnras/staf013> arXiv:2404.08052 [astro-ph.GA]
- [62] Bezanson, R., Labbe, I., Whitaker, K.E., Leja, J., Price, S.H., Franx, M., Brammer, G., Marchesini, D., Zitrin, A., Wang, B., Weaver, J.R., Furtak, L.J., Atek, H., Coe, D., Cutler, S.E., Dayal, P., van Dokkum, P., Feldmann, R., Förster Schreiber, N.M., Fujimoto, S., Geha, M., Glazebrook, K., de Graaff, A., Greene, J.E., Juneau, S., Kassin, S., Kriek, M., Khullar, G., Maseda, M., Mowla, L.A., Muzzin, A., Nanayakkara, T., Nelson, E.J., Oesch, P.A., Pacifici, C., Pan, R., Papovich, C., Setton, D.J., Shapley, A.E., Smit, R., Stefanon, M., Taylor, E.N., Williams, C.C.: The JWST UNCOVER Treasury Survey: Ultradeep NIRSpect and NIRCams Observations before the Epoch of Reionization. ApJ **974**(1), 92 (2024) <https://doi.org/10.3847/1538-4357/ad66cf> arXiv:2212.04026 [astro-ph.GA]
- [63] Arrabal Haro, P., Dickinson, M., Finkelstein, S.L., Kartaltepe, J.S., Donnan, C.T., Burgarella, D., Carnall, A.C., Cullen, F., Dunlop, J.S., Fernández, V., Fujimoto, S., Jung, I., Krips, M., Larson, R.L., Papovich, C., Pérez-González, P.G., Amorín, R.O., Bagley, M.B., Buat, V., Casey, C.M., Chworowsky, K., Cohen, S.H., Ferguson, H.C., Giavalisco, M., Huertas-Company, M., Hutchison, T.A., Kocevski, D.D., Koekemoer, A.M., Lucas, R.A., McLeod, D.J., McLure, R.J., Pirzkal, N., Seillé, L.-M., Trump, J.R., Weiner, B.J., Wilkins, S.M., Zavala, J.A.: Confirmation and refutation of very luminous galaxies in the early Universe. Nature **622**(7984), 707–711 (2023) <https://doi.org/10.1038/s41586-023-06521-7> arXiv:2303.15431 [astro-ph.GA]
- [64] Williams, H., Kelly, P.L., Chen, W., Brammer, G., Zitrin, A., Treu, T., Scarlata, C., Koekemoer, A.M., Oguri, M., Lin, Y.-H., Diego, J.M., Nonino, M., Hjorth, J., Langeroodi, D., Broadhurst, T., Rogers, N., Perez-Fournon, I., Foley, R.J., Jha, S., Filippenko, A.V., Strolger, L., Pierel, J., Poidevin, F., Yang, L.: A magnified compact galaxy at redshift 9.51 with strong nebular emission lines. Science **380**(6643), 416–420 (2023) <https://doi.org/10.1126/science.adf5307> arXiv:2210.15699 [astro-ph.GA]
- [65] Castellano, M., Napolitano, L., Fontana, A., Roberts-Borsani, G., Treu, T., Vanzella, E., Zavala, J.A., Arrabal Haro, P., Calabrò, A., Llerena, M., Mascia, S., Merlin, E., Paris, D., Pentericci, L., Santini, P., Bakx, T.J.L.C., Bergamini, P., Cupani, G., Dickinson, M., Filippenko, A.V., Glazebrook, K., Grillo, C., Kelly, P.L., Malkan, M.A., Mason, C.A., Morishita, T., Nanayakkara, T., Rosati, P.,

- Sani, E., Wang, X., Yoon, I.: JWST NIRSpec Spectroscopy of the Remarkable Bright Galaxy GHZ2/GLASS-z12 at Redshift 12.34. *ApJ* **972**(2), 143 (2024) <https://doi.org/10.3847/1538-4357/ad5f88> arXiv:2403.10238 [astro-ph.GA]
- [66] Eisenstein, D.J., Johnson, B.D., Robertson, B., Tacchella, S., Hainline, K., Jakobsen, P., Maiolino, R., Bonaventura, N., Bunker, A.J., Cameron, A.J., Cargile, P.A., Curtis-Lake, E., Hausen, R., Puskás, D., Rieke, M., Sun, F., Willmer, C.N.A., Willott, C., Alberts, S., Arribas, S., Baker, W.M., Baum, S., Bhatawdekar, R., Carniani, S., Charlot, S., Chen, Z., Chevallard, J., Curti, M., DeCoursey, C., D'Eugenio, F., de Graaff, A., Egami, E., Helton, J.M., Ji, Z., Jones, G.C., Kumari, N., Lützgendorf, N., Laseter, I., Looser, T.J., Lyu, J., Maseda, M.V., Nelson, E., Parlanti, E., Rauscher, B.J., Rawle, T., Rieke, G., Rix, H.-W., Rujopakarn, W., Sandles, L., Saxena, A., Scholtz, J., Sharpe, K., Shivaee, I., Simmonds, C., Smit, R., Topping, M.W., Übler, H., Venturi, G., Williams, C.C., Witstok, J., Woodrum, C.: The JADES Origins Field: A New JWST Deep Field in the JADES Second NIRCам Data Release. arXiv e-prints, 2310–12340 (2023) <https://doi.org/10.48550/arXiv.2310.12340> arXiv:2310.12340 [astro-ph.GA]
- [67] Yang, G., Boquien, M., Buat, V., Burgarella, D., Ciesla, L., Duras, F., Stalevski, M., Brandt, W.N., Papovich, C.: X-CIGALE: Fitting AGN/galaxy SEDs from X-ray to infrared. *MNRAS* **491**(1), 740–757 (2020) <https://doi.org/10.1093/mnras/stz3001> arXiv:2001.08263 [astro-ph.GA]
- [68] Prevot, M.L., Lequeux, J., Maurice, E., Prevot, L., Rocca-Volmerange, B.: The typical interstellar extinction in the Small Magellanic Cloud. *A&A* **132**, 389–392 (1984)
- [69] Lyu, J., Rieke, G.H.: Polar Dust, Nuclear Obscuration, and IR SED Diversity in Type-1 AGNs. *ApJ* **866**(2), 92 (2018) <https://doi.org/10.3847/1538-4357/aae075> arXiv:1809.03080 [astro-ph.GA]
- [70] Buat, V., Mountrichas, G., Yang, G., Boquien, M., Roehlly, Y., Burgarella, D., Stalevski, M., Ciesla, L., Theulé, P.: Polar dust obscuration in broad-line active galaxies from the XMM-XXL field. *A&A* **654**, 93 (2021) <https://doi.org/10.1051/0004-6361/202141797> arXiv:2108.07684 [astro-ph.GA]
- [71] Bruzual, G., Charlot, S.: Stellar population synthesis at the resolution of 2003. *MNRAS* **344**(4), 1000–1028 (2003) <https://doi.org/10.1046/j.1365-8711.2003.06897.x> arXiv:astro-ph/0309134 [astro-ph]
- [72] Calzetti, D., Armus, L., Bohlin, R.C., Kinney, A.L., Koornneef, J., Storchi-Bergmann, T.: The Dust Content and Opacity of Actively Star-forming Galaxies. *ApJ* **533**(2), 682–695 (2000) <https://doi.org/10.1086/308692> arXiv:astro-ph/9911459 [astro-ph]
- [73] Ciesla, L., Charmandaris, V., Georgakakis, A., Bernhard, E., Mitchell, P.D.,

- Buat, V., Elbaz, D., LeFloc'h, E., Lacey, C.G., Magdis, G.E., Xilouris, M.: Constraining the properties of AGN host galaxies with spectral energy distribution modelling. *A&A* **576**, 10 (2015) <https://doi.org/10.1051/0004-6361/201425252> [arXiv:1501.03672](https://arxiv.org/abs/1501.03672) [astro-ph.GA]
- [74] Carnall, A.C., McLure, R.J., Dunlop, J.S., Davé, R.: Inferring the star formation histories of massive quiescent galaxies with BAGPIPES: evidence for multiple quenching mechanisms. *MNRAS* **480**(4), 4379–4401 (2018) <https://doi.org/10.1093/mnras/sty2169> [arXiv:1712.04452](https://arxiv.org/abs/1712.04452) [astro-ph.GA]
- [75] Taylor, A.J., Finkelstein, S.L., Kocevski, D.D., Jeon, J., Bromm, V., Amorin, R.O., Arrabal Haro, P., Backhaus, B.E., Bagley, M.B., Bañados, E., Bhatawdekar, R., Brooks, M., Calabro, A., Chavez Ortiz, O.A., Cheng, Y., Cleri, N.J., Cole, J.W., Davis, K., Dickinson, M., Donnan, C., Dunlop, J.S., Ellis, R.S., Fernandez, V., Fontana, A., Fujimoto, S., Giavalisco, M., Grazian, A., Guo, J., Hathi, N.P., Holwerda, B.W., Hirschmann, M., Inayoshi, K., Kartaltepe, J.S., Khusanova, Y., Koekemoer, A.M., Kokorev, V., Larson, R.L., Leung, G.C.K., Lucas, R.A., McLeod, D.J., Napolitano, L., Onoue, M., Pacucci, F., Papovich, C., Pérez-González, P.G., Pirzkal, N., Somerville, R.S., Trump, J.R., Wilkins, S.M., Yung, L.Y.A., Zhang, H.: Broad-Line AGN at $3.5 < z < 6$: The Black Hole Mass Function and a Connection with Little Red Dots. *arXiv e-prints*, 2409–06772 (2024) <https://doi.org/10.48550/arXiv.2409.06772> [arXiv:2409.06772](https://arxiv.org/abs/2409.06772) [astro-ph.GA]
- [76] Newville, M., Otten, R., Nelson, A., Stensitzki, T., Ingargiola, A., Allan, D., Fox, A., Carter, F., Michał, Osborn, R., Pustakhod, D., Weigand, S., Ineuhaus, Aristov, A., Glenn, Mark, mgunyho, Deil, C., Hansen, A.L.R., Pasquevich, G., Foks, L., Zobrist, N., Frost, O., Stuermer, Jaskula, J.-C., Caldwell, S., Eendebak, P., Pompili, M., Hedegaard Nielsen, J., Persaud, A.: *lmfit/lmfit-py*: 1.3.2. <https://doi.org/10.5281/zenodo.12785036>
- [77] Raftery, A.E.: Bayesian model selection in social research. *Sociological Methodology* **25**, 111–163 (1995). Accessed 2023-07-10
- [78] Kovačević-Dojčinović, J., Dojčinović, I., Lakićević, M., Popović, L.Č.: Tracing the outflow kinematics in Type 2 active galactic nuclei. *A&A* **659**, 130 (2022) <https://doi.org/10.1051/0004-6361/202141043> [arXiv:2112.11797](https://arxiv.org/abs/2112.11797) [astro-ph.GA]
- [79] de Graaff, A., Rix, H.-W., Carniani, S., Suess, K.A., Charlot, S., Curtis-Lake, E., Arribas, S., Baker, W.M., Boyett, K., Bunker, A.J., Cameron, A.J., Chevallard, J., Curti, M., Eisenstein, D.J., Franx, M., Hainline, K., Hausen, R., Ji, Z., Johnson, B.D., Jones, G.C., Maiolino, R., Maseda, M.V., Nelson, E., Parlanti, E., Rawle, T., Robertson, B., Tacchella, S., Übler, H., Williams, C.C., Willmer, C.N.A., Willott, C.: Ionised gas kinematics and dynamical masses of $z \gtrsim 6$ galaxies from JADES/NIRSpec high-resolution spectroscopy. *A&A* **684**, 87 (2024) <https://doi.org/10.1051/0004-6361/202347755> [arXiv:2308.09742](https://arxiv.org/abs/2308.09742) [astro-ph.GA]
- [80] Greene, J.E., Labbe, I., Goulding, A.D., Furtak, L.J., Chemerynska, I., Kokorev,

- V., Dayal, P., Volonteri, M., Williams, C.C., Wang, B., Setton, D.J., Burgasser, A.J., Bezanson, R., Atek, H., Brammer, G., Cutler, S.E., Feldmann, R., Fujimoto, S., Glazebrook, K., de Graaff, A., Khullar, G., Leja, J., Marchesini, D., Maseda, M.V., Matthee, J., Miller, T.B., Naidu, R.P., Nanayakkara, T., Oesch, P.A., Pan, R., Papovich, C., Price, S.H., van Dokkum, P., Weaver, J.R., Whitaker, K.E., Zitrin, A.: UNCOVER Spectroscopy Confirms the Surprising Ubiquity of Active Galactic Nuclei in Red Sources at $z \lesssim 5$. *ApJ* **964**(1), 39 (2024) <https://doi.org/10.3847/1538-4357/ad1e5f> [arXiv:2309.05714](https://arxiv.org/abs/2309.05714) [astro-ph.GA]
- [81] Wang, B., Leja, J., de Graaff, A., Brammer, G.B., Weibel, A., van Dokkum, P., Baggen, J.F.W., Suess, K.A., Greene, J.E., Bezanson, R., Cleri, N.J., Hirschmann, M., Labbé, I., Matthee, J., McConachie, I., Naidu, R.P., Nelson, E., Oesch, P.A., Setton, D.J., Williams, C.C.: RUBIES: Evolved Stellar Populations with Extended Formation Histories at $z \sim 7-8$ in Candidate Massive Galaxies Identified with JWST/NIRSpec. *ApJ* **969**(1), 13 (2024) <https://doi.org/10.3847/2041-8213/ad55f7> [arXiv:2405.01473](https://arxiv.org/abs/2405.01473) [astro-ph.GA]
- [82] Dalla Bontà, E., Peterson, B.M., Grier, C.J., Berton, M., Brandt, W.N., Ciroi, S., Corsini, E.M., Dalla Barba, B., Davies, R., Dehghanian, M., Edelson, R., Foschini, L., Gasparri, D., Ho, L.C., Horne, K., Iodice, E., Morelli, L., Pizzella, A., Portaluri, E., Shen, Y., Schneider, D.P., Vestergaard, M.: Estimating Masses of Supermassive Black Holes in Active Galactic Nuclei from the H α Emission Line. *arXiv e-prints*, 2410–21387 (2024) <https://doi.org/10.48550/arXiv.2410.21387> [arXiv:2410.21387](https://arxiv.org/abs/2410.21387) [astro-ph.GA]
- [83] Richards, G.T., Lacy, M., Storrie-Lombardi, L.J., Hall, P.B., Gallagher, S.C., Hines, D.C., Fan, X., Papovich, C., Vanden Berk, D.E., Trammell, G.B., Schneider, D.P., Vestergaard, M., York, D.G., Jester, S., Anderson, S.F., Budavári, T., Szalay, A.S.: Spectral Energy Distributions and Multiwavelength Selection of Type 1 Quasars. *ApJS* **166**(2), 470–497 (2006) <https://doi.org/10.1086/506525> [arXiv:astro-ph/0601558](https://arxiv.org/abs/astro-ph/0601558) [astro-ph]
- [84] Ren, W., Guo, H., Shen, Y., Silverman, J.D., Burke, C.J., Wang, S., Wang, J.: Prior-informed Active Galactic Nucleus Host Spectral Decomposition Using PyQSOFit. *ApJ* **974**(2), 153 (2024) <https://doi.org/10.3847/1538-4357/ad6e76> [arXiv:2406.17598](https://arxiv.org/abs/2406.17598) [astro-ph.GA]
- [85] Kokorev, V., Chisholm, J., Endsley, R., Finkelstein, S.L., Greene, J.E., Akins, H.B., Bromm, V., Casey, C.M., Fujimoto, S., Labbé, I., Larson, R.L.: Silencing the Giant: Evidence of AGN Feedback and Quenching in a Little Red Dot at $z = 4.13$. *arXiv e-prints*, 2407–20320 (2024) <https://doi.org/10.48550/arXiv.2407.20320> [arXiv:2407.20320](https://arxiv.org/abs/2407.20320) [astro-ph.GA]
- [86] Garg, P., Narayanan, D., Byler, N., Sanders, R.L., Shapley, A.E., Strom, A.L., Davé, R., Hirschmann, M., Lovell, C.C., Otter, J., Popping, G., Privon, G.C.: The BPT Diagram in Cosmological Galaxy Formation Simulations: Understanding

the Physics Driving Offsets at High Redshift. ApJ **926**(1), 80 (2022) <https://doi.org/10.3847/1538-4357/ac43b8> arXiv:2201.03564 [astro-ph.GA]